This is how much denser the lithosphere is than the asthenosphere

As a result of the increased density, the lithosphere sinks into the asthenosphere.

To find out how much it sinks we apply Archimedes principle, known in geology as the principle of isostasy.

Simple application: an iceberg in the ocean (or an icecube in a glass)

$$\rho_{ice} = 0.9\ \rho_{water} = 900\ kg/m^3$$

Ice expands upon freezing — a very unusual property

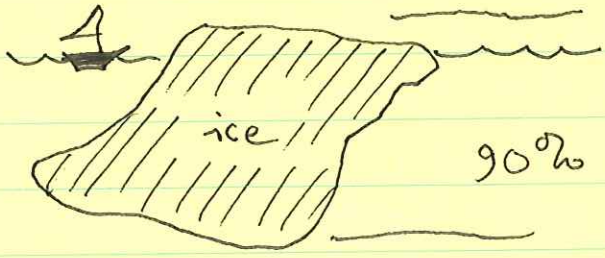

10% above — visible

90% below — this is why ship captains avoid icebergs

The principle of isostasy: equal mass in two columns

columns balancing →

$\rho_i \cdot d = \rho_w (d-h)$

$h = (1 - \frac{\rho_i}{\rho_w}) d$

$h = \frac{1}{10} d$

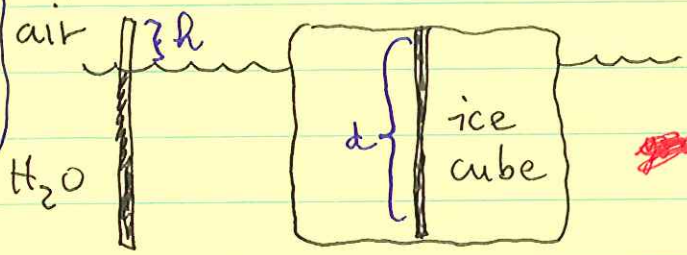

$\rho_{air} \approx 0$

need to draw similar sketch for Homework #3

Applied to the oceanic lithosphere
(note — heavy over light — inherently unstable — when lithosphere gets too old & heavy it subducts)

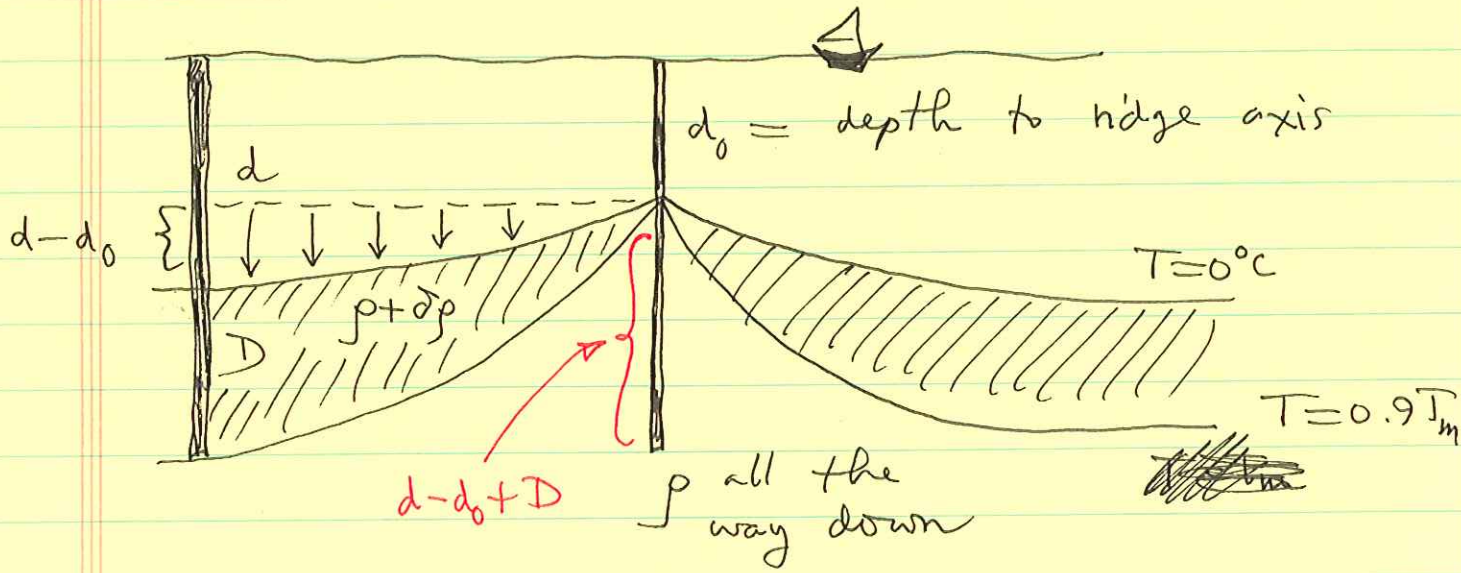

$$\underbrace{\rho_w d_0 + \rho (d - d_0 + D)}_{\text{ridge column}} \qquad \rho_w d_0 + \rho_m (d - d_0 + D)$$

$$= \rho_w d + \rho_m D + \int_0^D \delta\rho \, dz$$

$$= \underbrace{\rho_w d + (\rho + \delta\rho) D}_{\text{off-ridge}} \Rightarrow (\rho_m - \rho_w)(d - d_0) = \int_0^D \delta\rho \, dz = \int_0^\infty \delta\rho \, dz$$

see next page for simpler analysis

$$(\rho - \rho_w)\underbrace{(d - d_0)}_{\text{subsidence}} = \delta\rho\, D$$

↑ recall $\sim \sqrt{\text{age}}$

Note: by $\delta\rho$ we really mean the lithosphere average:

$$\overline{\delta\rho}\, D = \int_0^D \delta\rho\, dz$$

In fact, a more careful analysis shows that

$$\overline{\delta\rho} = \frac{2}{2.32\sqrt{\pi}}\, \rho\alpha T_M \approx 0.49\, \rho\alpha T_m$$

$\overline{\delta\rho}/\rho \approx 2\%$ corresponds to cooling by $\sim 50\%$ $1350^\circ \rightarrow 700^\circ C$

$$\frac{(.02)(3300)}{3300 - 1000} = \frac{70}{2300}$$

$$d = d_0 + \left(\frac{\overline{\delta\rho}}{\rho - \rho_w}\right) D$$

$$d = d_0 + 2\left(\frac{\rho}{\rho - \rho_w}\right) \alpha T_m \sqrt{\frac{kt}{\pi}}$$

$$d = d_0 + \frac{350\ \text{m}}{\sqrt{\text{age in m.y.}}}$$

An amazingly simple formula predicting ocean depths!

1 m.y. old lithosphere — very near the ridge has subsided by 350 m due to thermal contraction.

100 m.y. old lithosphere has subsided by 3.5 km.

How is ocean depth measured — with acoustic pingers aboard surface ships. Speed of sound in seawater 1500 m/sec.

Spreading rates & age of ocean crust can be determined using magnetic anomalies, as we shall see later.

discuss this after showing Reykjanes and other profiles

For a careful comparison it is necessary to correct for <u>sediment thickness</u> (since $\rho_{seds} \neq \rho_{basalt}$ or peridotite)

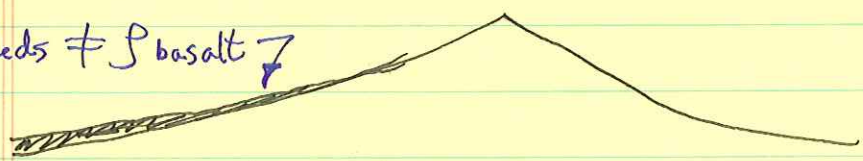

sed thickness — due to dead organisms increases with age — also affected by river influx — where correction most important

Isostatic geoid anomalies over the oceanic lithosphere

The oceanic lithosphere as it spreads away from mid-ocean ridge axes cools off and subsides due to thermal contraction.

We wish to calculate expected geoid height anomaly due to this phenomenon.

Since isostasy involves only uppermost regions of $\oplus$, we consider a locally flat model:

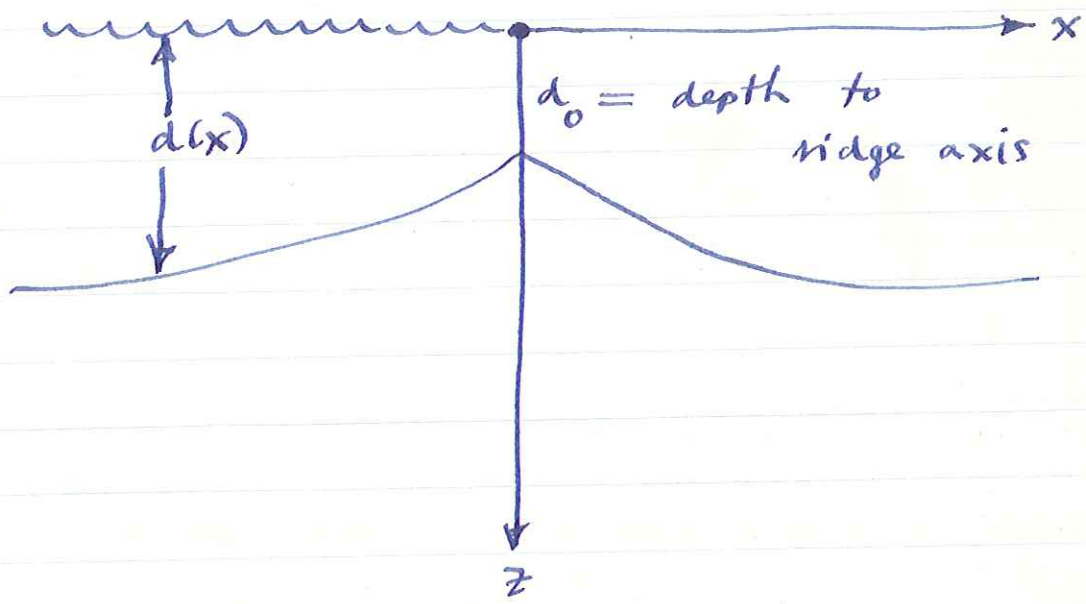

Sea H_2O density $\rho_w = 1.025 \sim 1$ gm/cm^3 ← greater than 1 (salty)

Standard column at ridge axis

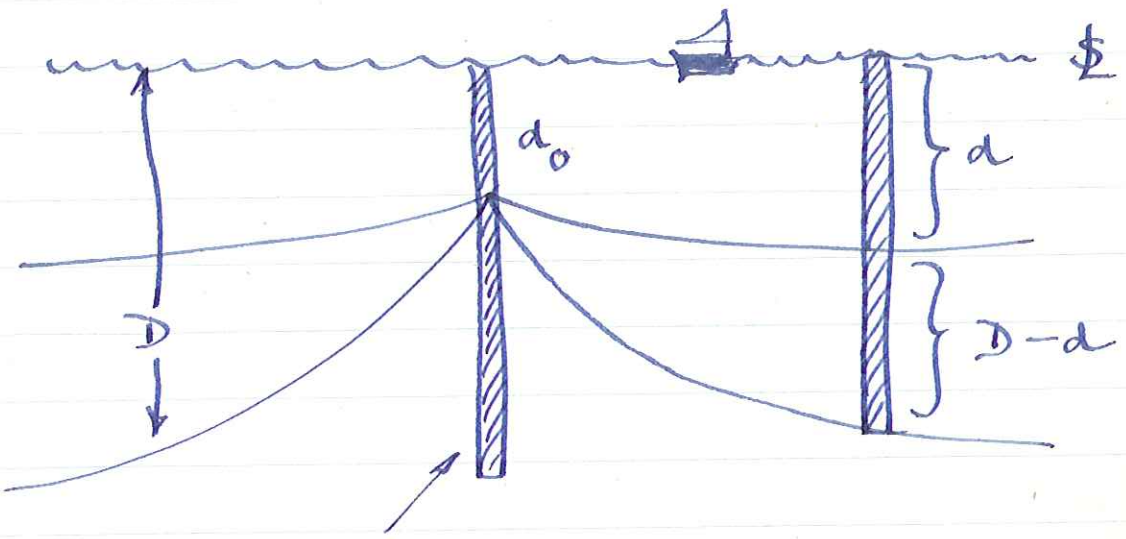

Significant cooling has occurred down to a depth D (compensation depth). We'll eventually let $D \to \infty$.

Two approximations will be made:

1. $d \ll D$, subsidence $\ll$ depth down to which cooling has occurred.

2. $D \ll L$, depth scale $\ll$ horizontal scale L over which $\exists$ significant lateral variations.

These 2 approx. are valid since, as we shall see, $d \sim 4$ km, $D \sim 100$ km and $L \sim 1000$ km. ($d - d_0 \approx 2$ km)

The approx. $D \ll L$ limits consideration to features (such as subsidence away from ridge) of broad horizontal scale (for which local isostasy a good approx.)

Anomalous density in $d < z < D$:
$\delta\rho(x, z)$ so total density is
$\rho_m + \delta\rho(x, z)$
$\delta\rho$ positive due to thermal contraction.

What is condition for isostatic balance?
Two shaded columns must have equal mass / cm^2.
Consider 1 cm^2 cross-sectional area.

Ridge column mass $= \rho_w d_0 + \rho_m (D - d_0)$

Flank column mass $= \rho_w d$

$$+ \int_d^D (\rho_m + \delta\rho)\, dz$$

$$= \rho_w d + \rho_m (D - d) + \int_0^D \delta\rho \, dz$$

can replace ↑ by zero with second order error as both d and $\delta\rho$ first order.

$$= \overbrace{\rho_w d_0 + \rho_m (D - d_0)}^{\text{same as ridge column}} + \underbrace{(\rho_w - \rho_m)(d - d_0) + \int_0^D \delta\rho \, dz}_{\text{must vanish}}$$

$$\boxed{(\rho_m - \rho_w)(d - d_0) = \int_0^\infty \delta\rho(x,z) \, dz}$$

Relates <u>subsidence</u> $d(x) - d_0$ away from ridge to <u>anomalous</u> density in cooling lithosphere.

Now what is the geoid signal? A slightly tricky argument is required to find this. We seek the anomalous grav. potential $V(x)$ on $\mathcal{L}$, the level $z = 0$.

We integrate over rings of mass below the observation point:

call this δV

find V here (say)

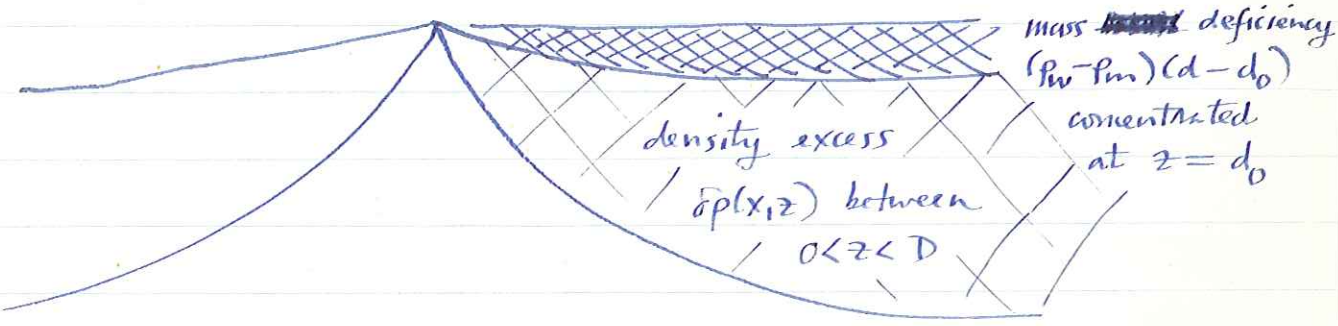

We consider the model (cylindrical coords centered on obs. pt.)

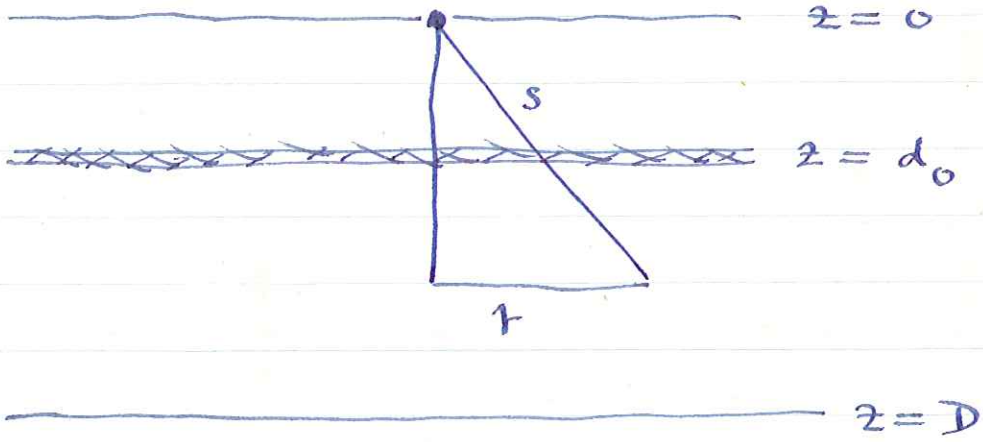

Rings: all pts. same dist. s from.

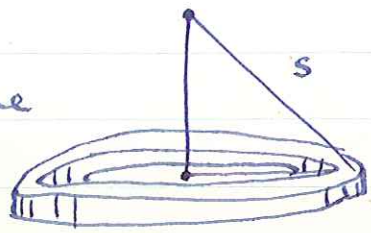

Integrate out a distance L.

$s = \sqrt{r^2 + z^2}$, ϕ = azimuthal angle

Then

call this δV

$$V = -G \int_0^{2\pi} \int_0^{L} \frac{(\rho_w - \rho_m)(d - d_0)}{\sqrt{r^2 + d_0^2}} \, r \, dr$$

$$- G \int_0^{2\pi} \int_{d_0}^{D} dz \int_0^{L} \frac{\delta\rho(x,z)}{\sqrt{r^2 + z^2}} \, r \, dr$$

Top integral :

$$- 2\pi G \int_0^{L} \frac{(\rho_w - \rho_m)(d - d_0)}{\sqrt{r^2 + d_0^2}} \, r \, dr$$

Since integral only out to $r = L$ = distance over which d, $\delta\rho$ change insignificantly, can take d = const and $\delta\rho$ = const

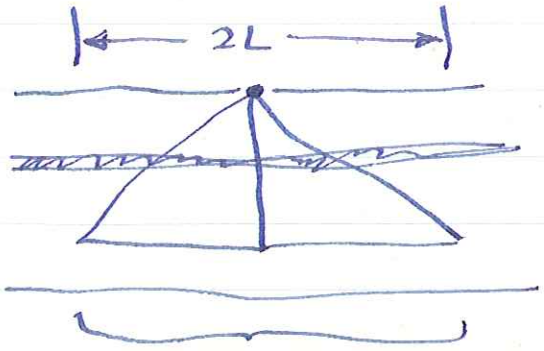

lithosphere looks the same in this region since $D \ll L$.

Let $u^2 = r^2 + d_0^2$

$u\,du = r\,dr$

top integral $= -2\pi G(\rho_w - \rho_m)(d-d_0)\left[\sqrt{L^2+d_0^2} - d_0\right]$

to next order this is $L + \frac{d_0}{2L}$

$\approx -2\pi G(\rho_w - \rho_m)(d-d_0)\,L$ ← since $d_0 \ll L$

bottom integral $= -2\pi G$ [redacted] $\int_{d_0}^{D} \delta\rho\, dz$ ← make this ∞

$\int_0^L \frac{r\,dr}{\sqrt{r^2+z^2}}$ ← have already replaced by zero

can't just replace this by L as above since z can be much larger than d_0.

$= -2\pi G \int_{d_0}^{D} \delta\rho \left[\sqrt{L^2+z^2} - z\right] dz$ ← $D \to \infty$

← can replace by 0 as before (actually, we've already done so)

Now since $D \ll L$ we know that $z \ll L$ so

$\sqrt{L^2+z^2} \approx$ [redacted] $L + \frac{z^2}{2L} + \cdots$

bottom integral $\approx -2\pi G L \int_0^D \delta\rho\, dz$ $D \to \infty$ here too

$-2\pi G \left(\frac{1}{2L}\right) \int_0^D z^2\, \delta\rho\, dz$

$+ 2\pi G \int_0^D z\, \delta\rho\, dz$

Altogether we get for $\delta V(x)$:

$$\delta V = 2\pi G L \left[(\rho_m - \rho_w)(d - d_0) - \int_0^D \delta\rho \, dz \right] + 2\pi G \int_0^D z \, \delta\rho \, dz - \pi G \int_0^D \frac{z^2}{L} \delta\rho \, dz + 2\pi G (\rho_M - \rho_W)(d - d_0) \frac{d_0^2}{2L}$$

The term $\propto L$ cancels exactly by the isostatic condition.

Isostasy is local; we are now free to take L as large as we desire, since the possibly troublesome term ($\propto L$) cancels out.

The third term is of relative order D/L compared to the second and can be neglected. Thus we get, finally,

$$\delta V(x) = 2\pi G \int_0^D z \, \delta\rho(x, z) \, dz$$

(can now let this depend on x again)

What is the corresponding geoid height anomaly?

In the absence of cooling and subsidence the potential due to

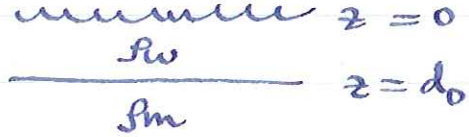

is, say, $V_0(z)$. On the $\oint$ $V_0(z) = V_0(0)$ = const., as $\oint$ is an equipotential.

With cooling and subsidence $\oint$ gets displaced away from $z = 0$ by an amount $h(x)$ but keeps the same potential $V_0(0) =$ const. Thus.

$$V_0(0) = V_0(h) + \delta V(h) = \text{const.}$$

δV ← anomalous or extra potential just calculated

Taylor series:

Picture:

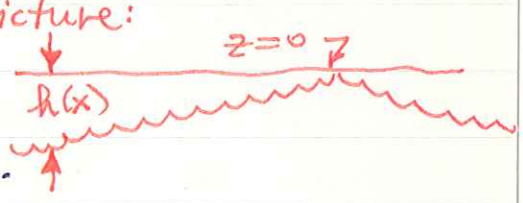

$$V_0(0) = V_0(0) + h V'(0) + \cdots + \delta V(0) + \cdots$$

Neglect .... terms. Now note that $V'(0) \equiv (dV_0/dz)_{z=0} = -g_0 =$ accel. of gravity at level $z = 0$ $= 980$ cm/s^2.

Thus the geoid elevation w.r.t. $z = 0$ (flat ≡ actually, the hydrostatic ellipsoid) is given by

$$h(x) = + \frac{1}{g_0} V(0,x) \Big|_{z=0}$$

— if $h(x)$ is measured positive downwards

or, finally,

$$h(x) = +(2\pi G/g_0) \underbrace{\int_0^D z\, \delta\rho(x,z)\, dz}$$

note: geoid signal at any point depends only on mass distr. below that point if DKL. lithospheric density

dipole moment of anomalous

Summarized by Turcotte & Schubert pp. 522-29

This relation between h and the local dipole moment of the [redacted] density anomaly, in the case of an isostatically compensated density distribution due to Turcotte + Ockendon JGR (1977).

We shall make use of it in a moment.

This often taken to be the definition of the lithosphere thickness — thermal boundary layer — whether 95 % or some other % is arbitrary.

How do we calculate the subsidence and the geoid anomaly.

Because of thermal contraction the cooled region becomes more dense than the ambient mantle density ρ_m.

The anomalous density with depth as a function of age is

$$\delta\rho(z,t) = \rho_m \alpha \left[T_m - T(z,t) \right]$$

where α is the (volumetric) thermal expansion coefficient.

defn: α = fractional increase in volume $\delta V / V$ of a sample due to a 1°C. rise in temperature.

An increase in volume corresponds to a decrease in density $\delta\rho / \rho_m = - \delta V / V$

A typical value of α for igneous rocks is $\alpha \sim 3 \cdot 10^{-5}$ / °C.

Cooling by 1000 °C. thus increases the density by 3% from $\rho_m = 3.33$ g/cm^3 to 3.43 gm/cm^3. This is about how much <u>denser</u> the lithosphere is than the asthenosphere.

Note the <u>inherent instability</u> of the lithosphere. The isostatic balance is the opposite of that usually considered, e.g. an iceberg

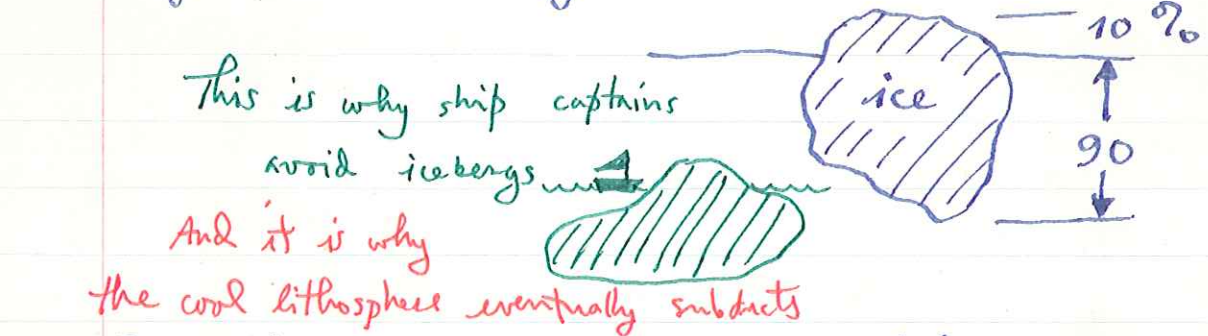

This is why ship captains avoid icebergs

And it is why the cool lithosphere eventually subducts

But in case of <u>oceanic lithosphere</u>:

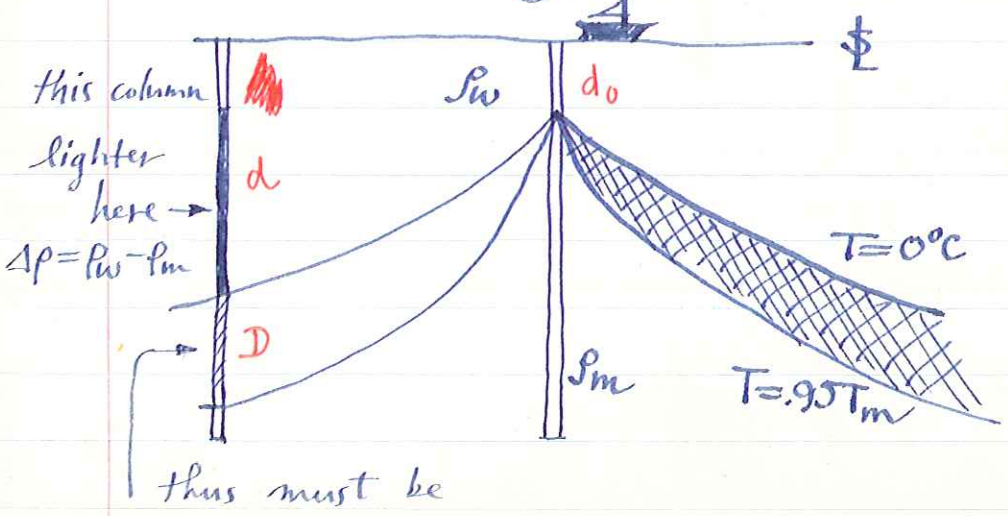

thus must be heavier here

This unstable situation thought to be one of the main <u>driving forces</u> of plate tectonics.

$$\delta\rho = \rho_m \alpha T_m \underbrace{\left[1 - \text{erf}\left(z/\sqrt{4kt}\right)\right]}$$

this called erfc: complementary error function

$$\boxed{\delta\rho(z,t) = \rho_m \alpha T_m \, \text{erfc}\left(z/\sqrt{4kt}\right)}$$

Plot of erfc looks like

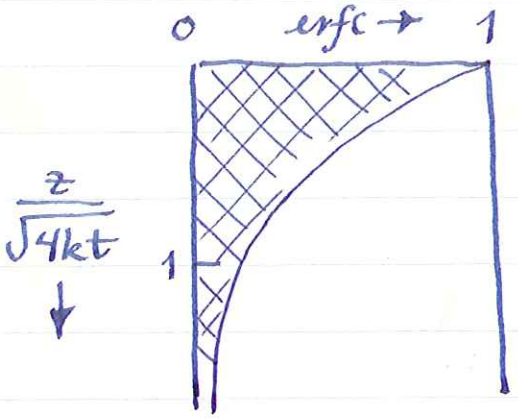

picture of anomalous density: greatest at top decreases with depth

By isostatically balancing columns we derived the formula for the subsidence

we now take D to be ∞

$$(\rho_m - \rho_w)(d - d_0) = \int_0^{\infty} \delta\rho(x,z)\, dz$$

Alternatively we could have taken the solution

$$T(z,t) = T_m \operatorname{erf}\left(\frac{z-d}{\sqrt{4kt}}\right)$$

This would satisfy upper b.c. at $z = d$ rather than $z = 0$. But these are nicetie's.

$$\int_0^\infty \delta\rho \, dz = \rho_m \alpha T_m \int_0^\infty \operatorname{erfc}\left(\frac{z}{\sqrt{4kt}}\right) dz$$

$$= \rho_m \alpha T_m (4kt)^{1/2} \int_0^\infty \operatorname{erfc} u \, du$$

$$u = \frac{z}{\sqrt{4kt}}$$

$$dz = \sqrt{4kt}\, du$$

The integral is just the shaded area.

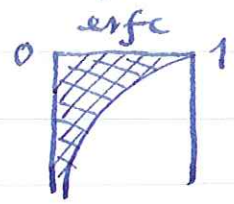

Can be shown that

$$\int_0^\infty \operatorname{erfc} u \, du = \frac{1}{\sqrt{\pi}}$$

Thus we get

$$d = d_0 + 2\left(\frac{\rho_m}{\rho_m - \rho_w}\right) \alpha T_m \left(\frac{kt}{\pi}\right)^{1/2}$$

The subsidence of the seafloor should vary as $t^{1/2}$ where t is the age.

This is an incredibly simple prediction for such a complicated tectonic process as sea-floor spreading must be.

Essentially the $t^{1/2}$ dependence comes from fact that thickness of cooled layer goes like $t^{1/2}$ and subsidence depends on thermal contraction.

For the geoid signal, relative to the rise crest, we derived the formula

$$h = + \frac{2\pi G}{g} \underbrace{\int_0^\infty z\, \delta\rho\,(x,z)\, dz}$$

dipole moment of anomalous density.

$u = z/\sqrt{4kt}$

$$h = +(2\pi G/g) \int_0^\infty z \operatorname{erfc}(z/\sqrt{4kt})\, dz$$

$$= + \frac{2\pi G}{g} (4kt) \underbrace{\int_0^\infty u \operatorname{erfc} u \, du}_{\text{this definite integral has value } 1/4}$$

Thus

$$\boxed{h = + \frac{2\pi G}{g} \rho_m \alpha T_m k t}$$

The geoid anomaly is everywhere ~~negative~~ lower than at the ridge and $\propto$ age t.

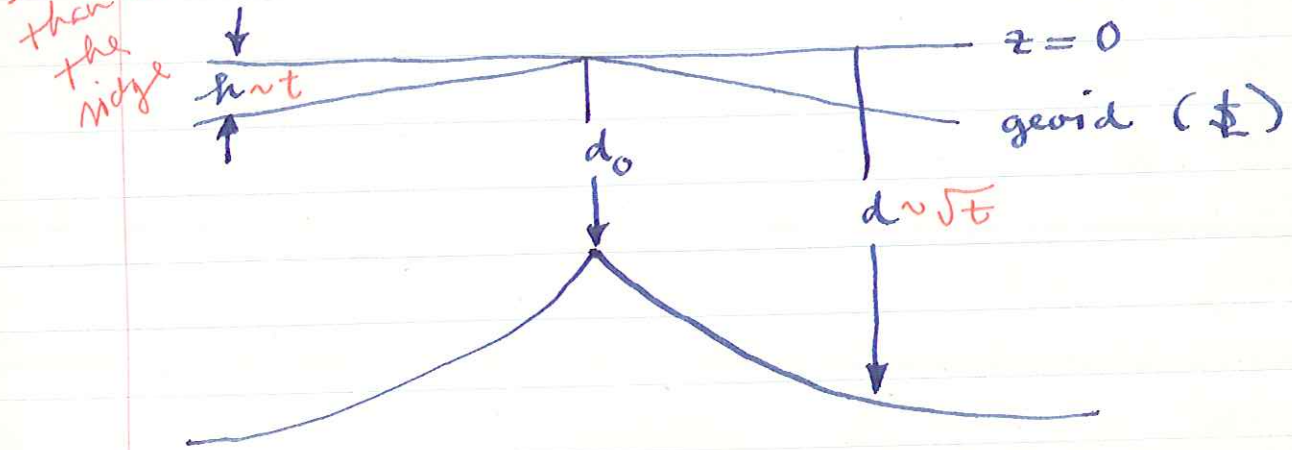

Picture highly distorted since actually $h \ll d$.

The lab exercise writes

$$d - d_0 = c_1 \sqrt{t}$$
$$h = + c_2 t$$

where c_1 is as we have derived and

$$c_2 = \frac{2\pi G}{g} \rho_m \alpha (T_m - T_0) \kappa \left[1 + \frac{2\rho_m \alpha (T_m - T_0)}{(\rho_m - \rho_w)\pi} \right]$$

here T_0, the upper temp not necessarily zero

this factor extra has value 1.04

The difference comes from a slightly different point of view (actually due to integrating z times $\Delta\rho = \rho_w - \rho_m$ in region $d_0 < z < d$). Extra factor of 1.04 is significant compared to measurement error.

Using "typical" values (those adopted by Parsons and Sclater 1977)

$\alpha = 3.2 \cdot 10^{-5}$ °C^{-1}
$T_m = 1350$ °C.
$\kappa = 0.008$ cm^2/s
$\rho_m = 3.33$ g/cm^3
$\rho_w = 1.0$ g/cm^3
$g = 980$ cm/s^2

$$C_1 = 350 \text{ m} / (\text{m.y.})^{1/2}$$

$$C_2 = 0.15 \text{ m} / \text{m.y.}$$

How does this agree with observations? This is the object of the lab. exercise. Recent study of Heestand and Crough of depth vs. $(\text{age})^{1/2}$ tries to "correct" for hot spot bias by eliminating points near (within 1000 km) hotspots. Finds

$$d = 2800 \text{ m} + 320 \text{ m} / (\text{m.y.})^{1/2}$$

Also must correct for <u>sediment thickness</u>

(since they are not as dense as $\rho = 3.3$ lithosphere)

generally increases with age (more time for bugs to fall on top)

known from seismic profiling.

Haxby 1980 or 1981 study of GEOS-3 data from MAR + Reykjanes.

Here one must correct for broad regional geoid bumps (sources below lithosphere)

The h vs. t is seen very nicely and agrees very well with the prediction

$$h = 0.15 \text{ m} / (\text{m.y.})$$

15 m anomaly at 100 m.y.

This excellent agreement is very strong evidence for the isostatic compensation of the lithosphere. Even a small deviation from isostasy would affect this result significantly, as you'll see from homework problem.

Currently a controversy over whether d vs. $t^{1/2}$ continues out to very old basins (200 m.y.). If all data is considered, a flattening of d vs. $\sqrt{t}$ is seen beyond 80 m.y. Very old basins do not continue to subside. No longer cools like a half-space. Would imply an extra source of heat from below.

This phenomenon first described quantitatively by Parsons and Sclater 1977 who found $c_1 = 350$ m/m.y$^{1/2}$ out to 80 m.y.

But when hot-spot contamination corrected for might be like $\sqrt{t}$ for [redacted] even oldest basins. Trouble: in N. Atlantic studied by Heestand + Crough ∃ no old ocean floor far from hot spots.

One more measured quantity can be predicted by our model: the heat flow.

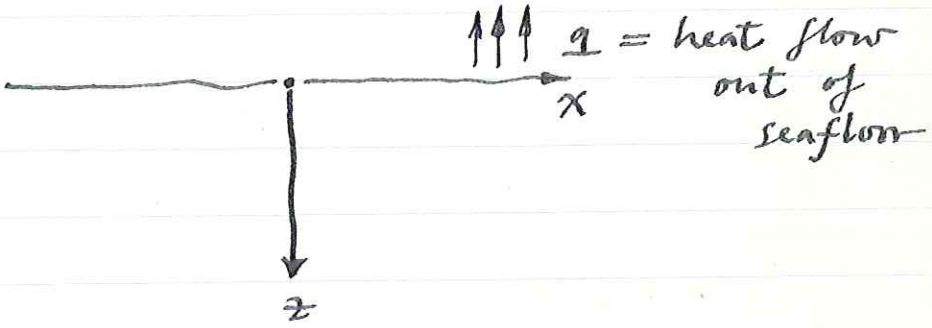

heat flow $q = \kappa \left(dT/dz\right)_{z=0}$

$$T = \frac{2}{\sqrt{\pi}} T_m \int_0^{z/\sqrt{4kt}} e^{-u^2}\, du$$

$$\frac{dT}{dz} = \frac{2}{\sqrt{\pi}} T_m \, e^{-z^2/4kt} \, (4kt)^{-1/2}$$

$$\left(dT/dz\right)_{z=0} = T_m \left(\pi k t\right)^{-1/2}$$

Thus we predict that, since $\kappa = \rho_m c_p k$,

$$\boxed{q = \rho_m c_p T_m (k/\pi t)^{1/2}}$$

The heat flow should vary like $t^{-1/2}$
The singularity at $t=0$ (the rise crest) shows that our solution breaks down very near the rise crest. Can be improved by modifying the b.c.

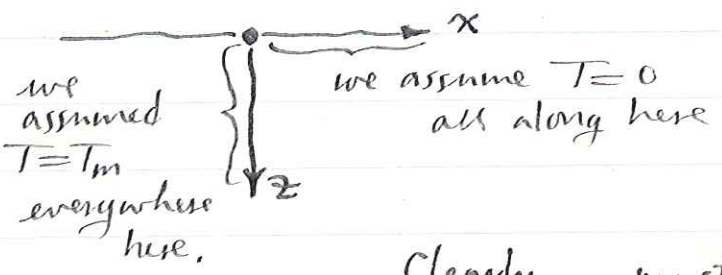

Clearly σ must exhibit some kind of singularity. This not only due to our approx. that heat flows only vertically. Need to modify b.c. on vertical axis.

But this effects soln only very near ridge (within the axial valley where active volcanism is occurring).
How does our solution compare with data elsewhere?

Recall the scatter and extreme local variability of measurements near the rise axis (ages < 30 – 40 m.y.).

Scatter most extreme in poorly sedimented areas. Sediment cover increases with age.

If averages of <u>all measurements</u> taken and plotted vs. age agreement with q vs. $t^{-1/2}$ is pretty good for $t > 30-40$ m.y. but poor for $t < 30-40$ m.y. (see pts ⊡, ⊙, ⧋ in Fig. 10 of Parsons + Sclater 1977). Theoretical <u>curve</u> uses values for ρ_m, c_p, k given previously.

Discrepancy for $t < 30-40$ m.y. and scatter now both attributed to <u>hydrothermal circulation</u> in basaltic oceanic crust.

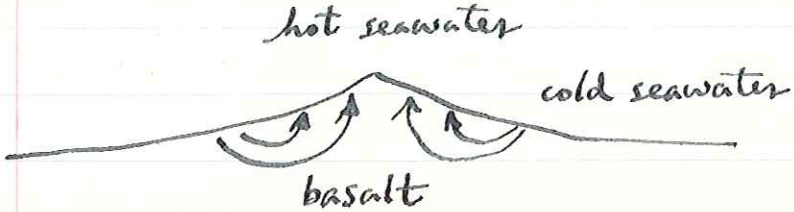

This can account for local variability.

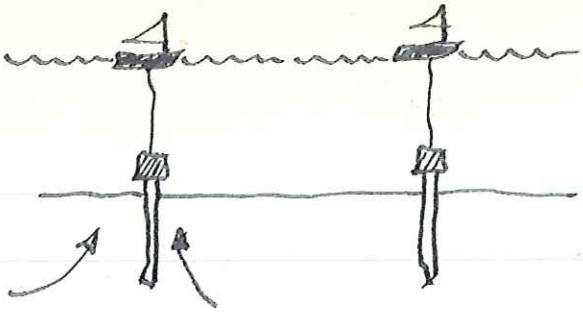

near hot spring: much of heat transported as hot H_2O, get a low measurement

not near hot spring: heat conduction dominates, get a reliable measurement

Only the conducted heat flow is measured.
The hot springs are thought to be most frequent in poorly sedimented areas.
Sediment cover seems to seal off cracks and vents in the basalt and influence the circulation.

If so-called "reliable" q averages are plotted (values in regions with uniform sed. cover > 200 m. thick) are plotted ⧫ the agreement is much better.

If take log:

$$\log q = \text{const} - 1/2 \log t$$

Slope of a log-log plot should be -1/2. The agreement, shown in Fig. 11 of P+S, is quite good from 5 to 150 m.y.

Existence of submarine hot springs first inferred on basis of heat flow measurements.

First direct evidence 1977 Alvin submersible found hydrothermal vents 2 locations

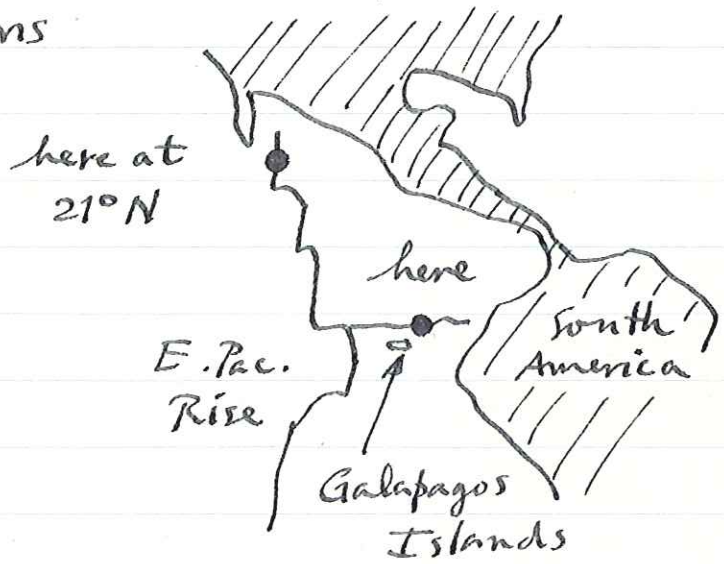

Hot springs on Galapagos Ridge 17°C.
" compared to 2°C. ambient bottom temp.
Black smokers" at 21°N however almost 400°C, kept from boiling by seabottom pressure. Galapagos vents diluted by cold seawater leakage from sides.

Interesting fauna, e.g. large red clots of hemoglobin because of low O_2 content) clams.

Can estimate amount of heat flowing out in form of hot H_2O by an argument based on Helium 3. Helium inert and very light, escapes from our atmosphere quickly, would not be in atmosphere unless constantly replenished. Most of this coming from oceanic hot springs.

one finds tail of Maxwell-Boltzmann distribution > escape velocity from ⊕

Can calculate rate of escape to space $\approx 3 \cdot 10^{19}$ atoms/sec. This much must be leaking out of ⊕ to keep atmospheric concentration in steady state.

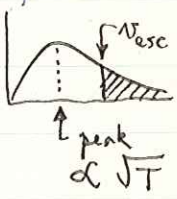

this ratio same for both cold Galapagos and hot 21°N; evidence for leaky plumbing of former.

Can measure ratio of He atoms / calorie in water samples collected by Hwin at vents ($8 \cdot 10^{-8}$ cal / atom of He 3)

$$3 \cdot 10^{19} \frac{\text{atoms}}{\text{sec}} \times 3 \cdot 10^{7} \frac{\text{sec}}{\text{yr}} \times 8 \cdot 10^{-8} \frac{\text{cal}}{\text{atom}}$$

Estimated heat escaping from all oceanic hot springs $7 \cancel{0} \cdot 10^{19}$ cal/yr
or about $\cancel{0}\ 10 \cdot 10^{12}$ W (J/sec)
10 Terrawatts

Can be compared with amount that "all data" averages fall below the theoretical heat flow

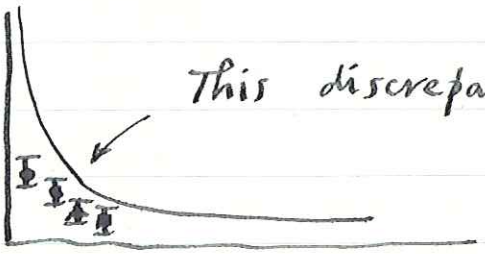

This discrepancy estimated by Langseth and Anderson to be $8 \cdot 10^{12}$ W in excellent (!) ~~reasonable~~ agreement with above estimate.

Importance of vents for oceanic chemistry is profound. From concentration of He 3 can estimate total flow of seawater through the crustal plumbing Get 6000 m^3/s, about 1/3 flow of Mississippi at New Orleans.

Entire ocean cycled through seafloor in 5–10 m.y. or about 500 times since world began. Many chemical exchanges occur during this cycling, solves many previously perplexing geochemical problems, e.g. known for years that conc. of Mg in oceans less than that flowing in in rivers. Reason: gets stripped out during cycling through crust.

Hot springs also a source of sulfide ore deposits. Iron, copper, other heavy metal sulfides utterly insoluble in H_2O at ordinary temps. but soluble in 400°C. The instant the water emerges and cools, sulfides precipitate out, "black smokers" are precipitating sulfides.

By viewing the films and videotapes of the "black smokers" one can estimate the total flow rate coming out of a single hydrothermal vent system.

At 21° N it is estimated to be $v = 1-5$ m/s and radius $r = 10-20$ cm. The total heat flow out the system is

$$q = \pi r^2 v \rho_w c_p T$$

(T: 350° – 400° C.)

$$\approx 6 \cdot 10^7 \text{ cal/sec}$$

The <u>total</u> hydrothermal heat flow, estimated from the ^3He / calories, is $5 \cdot 10^{19}$ cal/yr $\sim 1.7 \cdot 10^{12}$ cal/sec.

The estimated number of hydrothermal events required on all the world's ridge systems is thus about 25,000 – 30,000.

This is one for every 4–7 km of ridge length, which is why they're hard to find in the dark under 2.5 km of seawater.

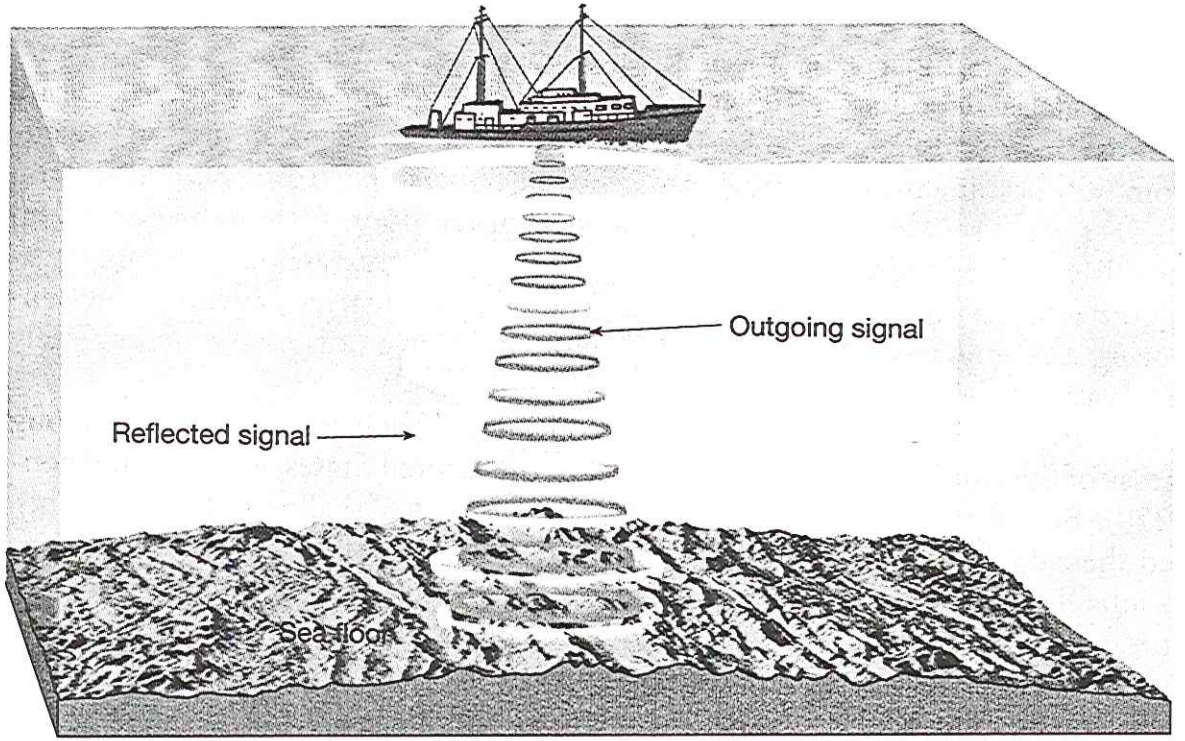

Figure 19.2 An echo sounde determines the water depth by measuring the time interval required for a sonic wave to tra from a ship to the sea floor and back. The speed of sound in w 1500 m/sec. Therefore, depth (1500 m/sec × echo travel time

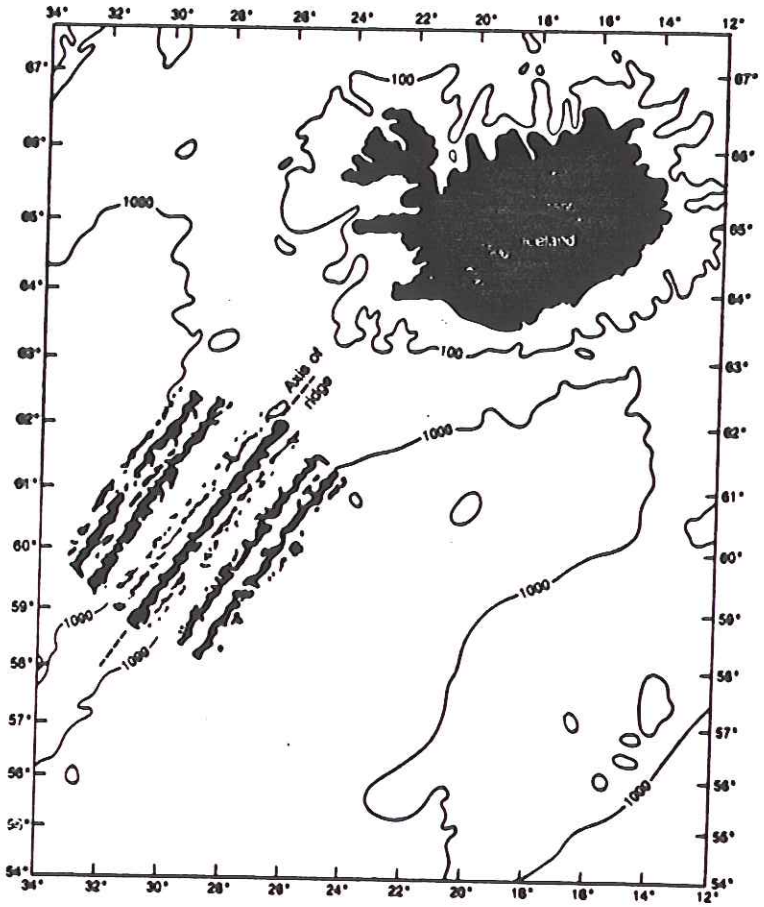
Iceland
Axis of ridge
100
1000

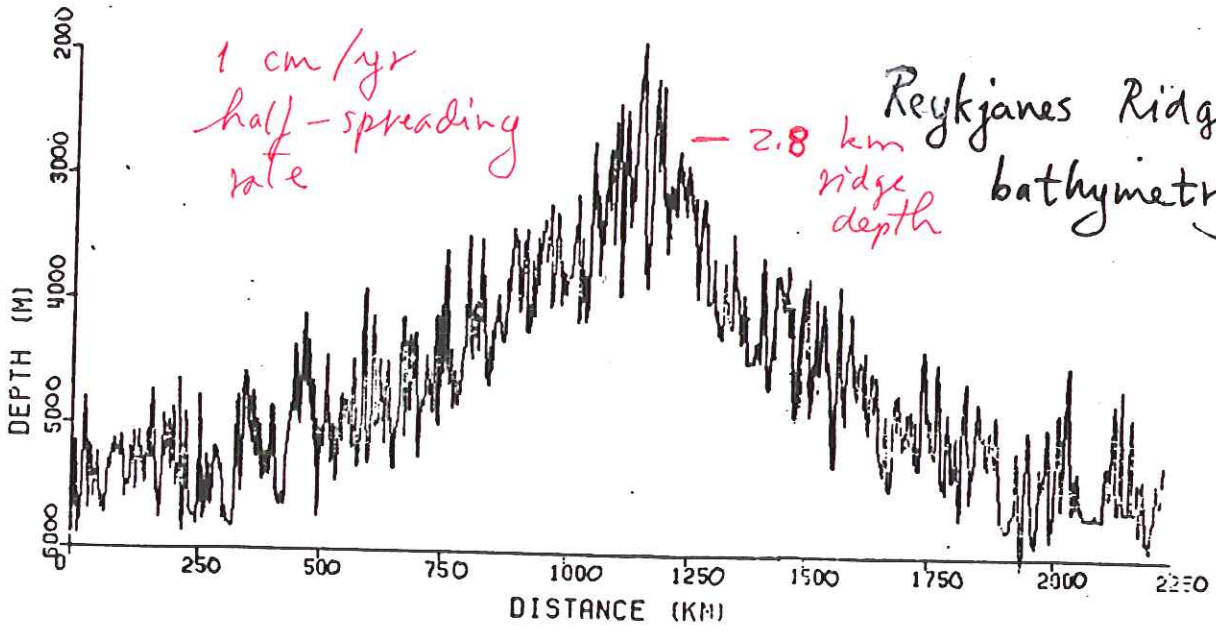
1 cm/yr
half-spreading
rate
2.8 km
ridge
depth
Reykjanes Ridge
bathymetry
DEPTH (M)
2000
3000
4000
5000
6000
250
500
750
1000
1250
1500
1750
2000
2250
DISTANCE (KM)

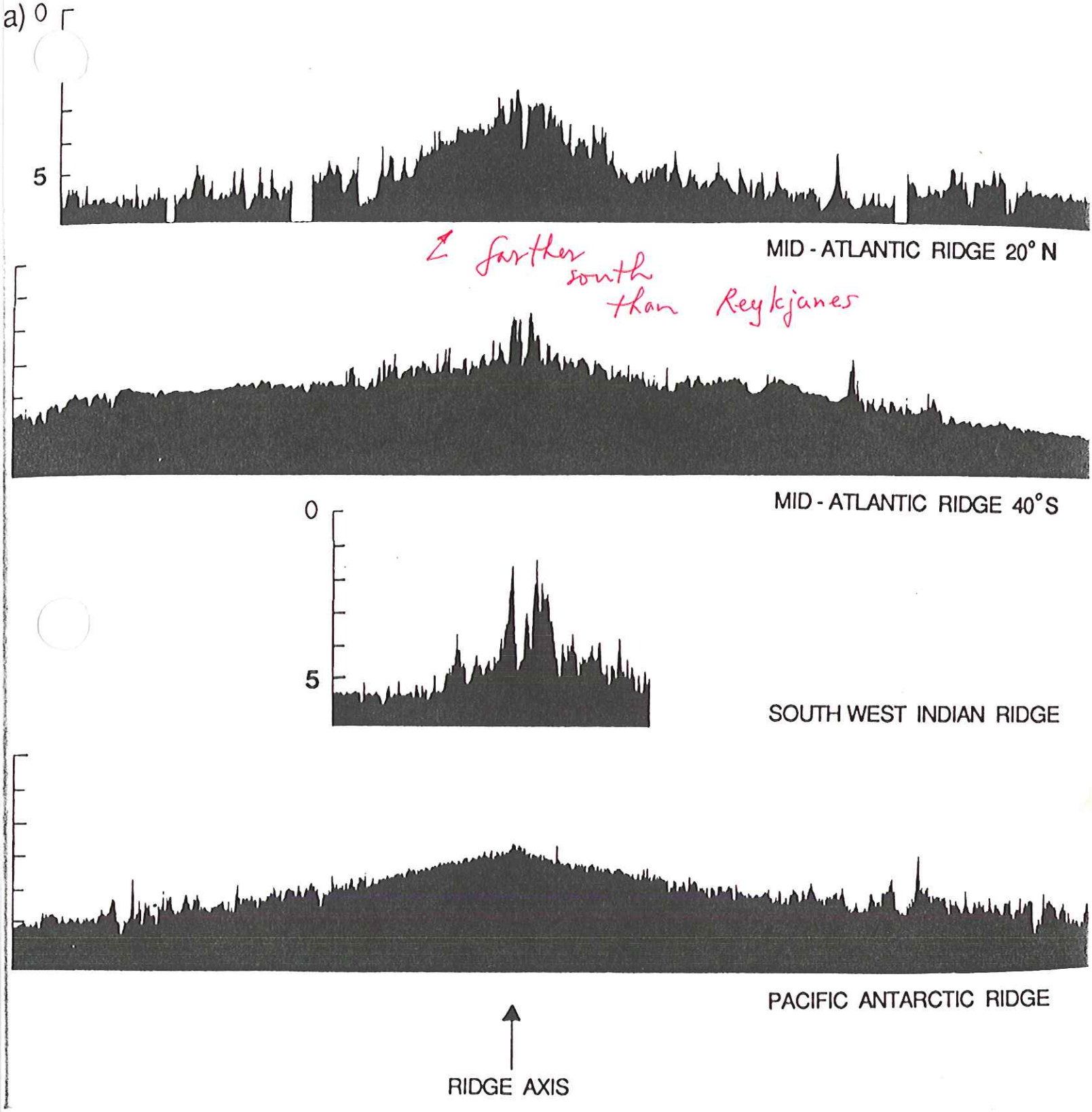
a) 0
5
MID - ATLANTIC RIDGE 20° N
farther south than Reykjanes
MID - ATLANTIC RIDGE 40°S
0
5
SOUTH WEST INDIAN RIDGE
PACIFIC ANTARCTIC RIDGE
RIDGE AXIS

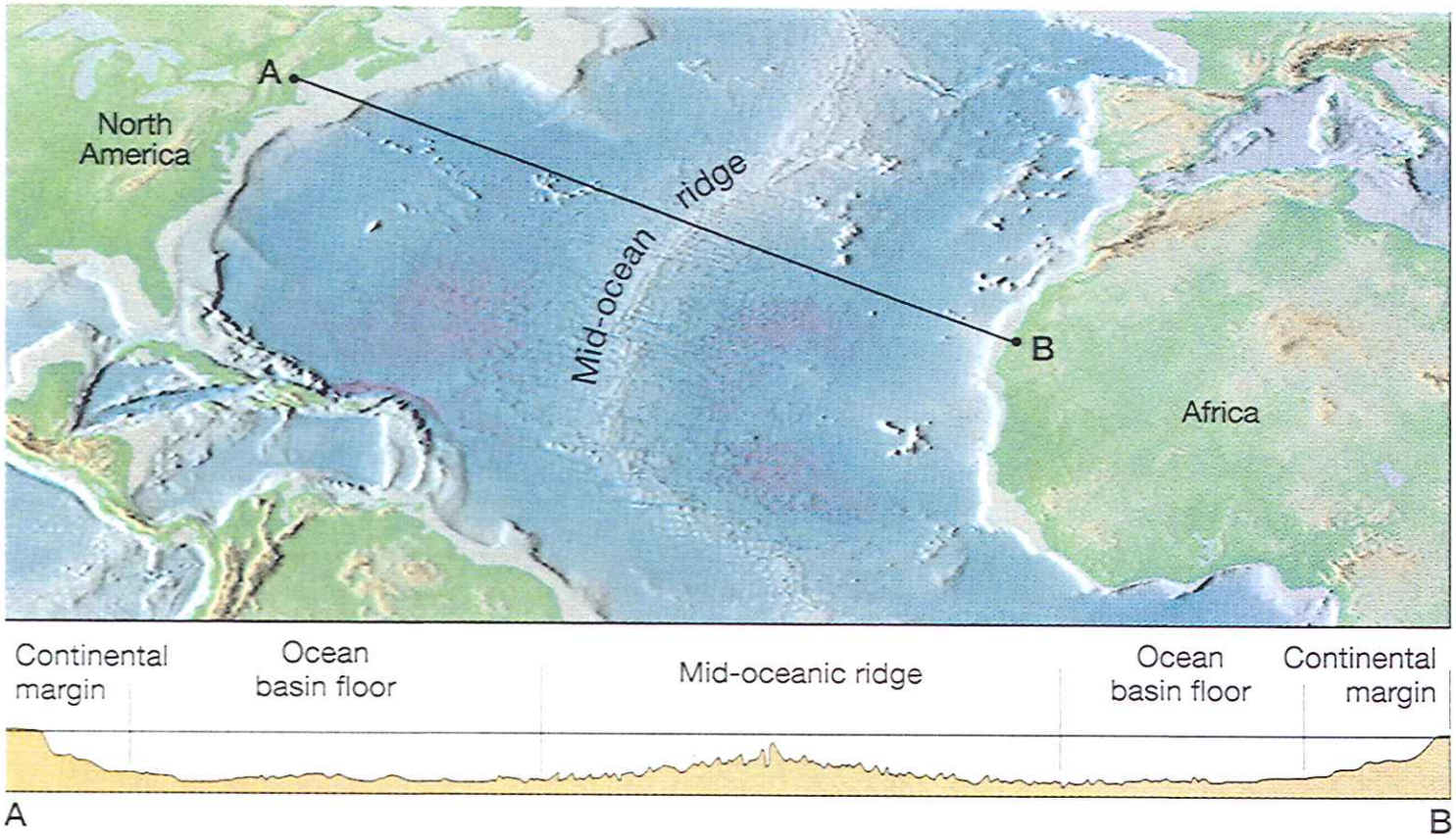
A
North America
Mid-ocean ridge
B
Africa
Continental margin
Ocean basin floor
Mid-oceanic ridge
Ocean basin floor
Continental margin
A
B

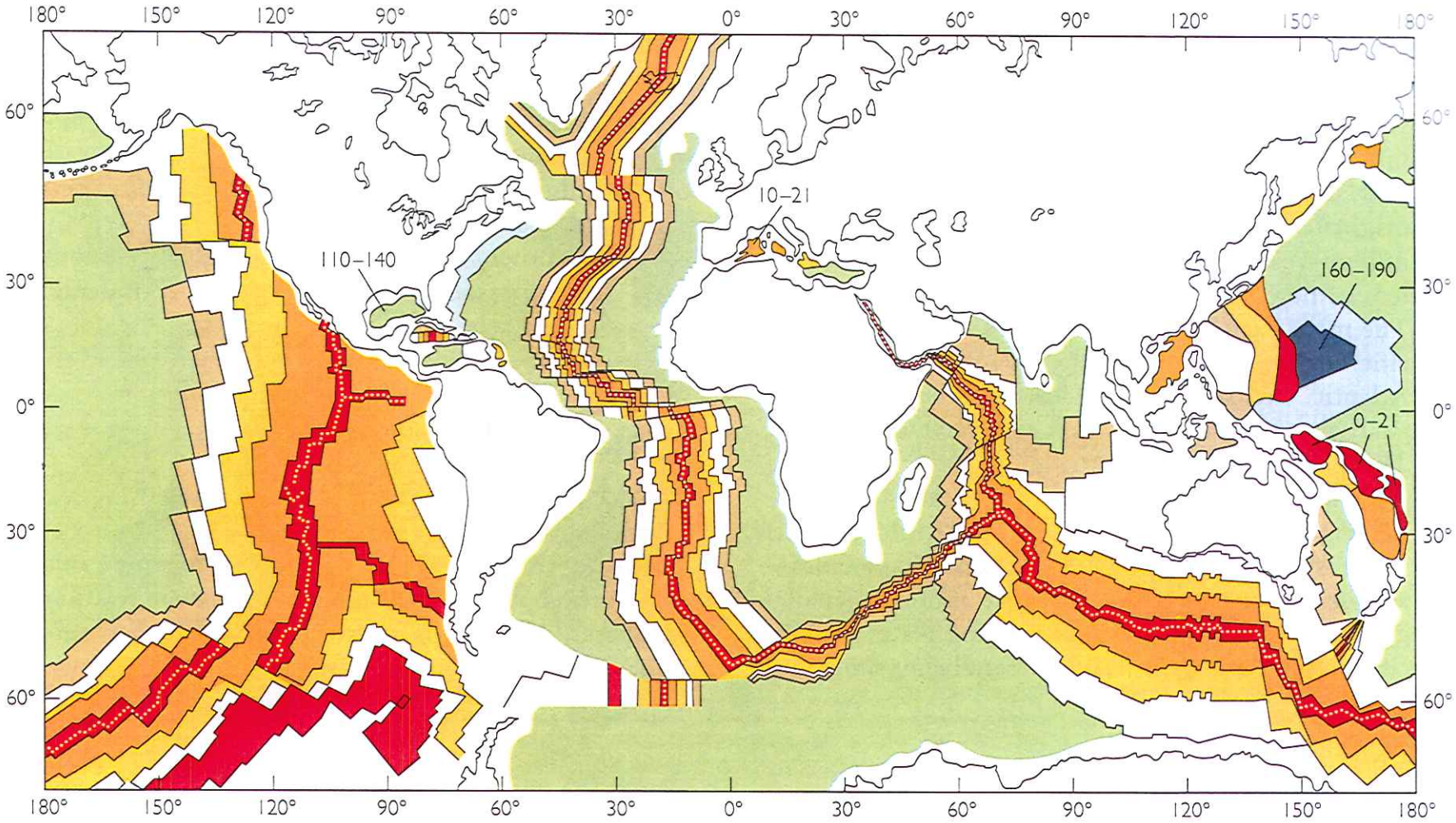

The age of the ocean basins (in millions of years)

0–5	Pleistocene–Pliocene	38–52	Eocene	140–160	Early Jurassic
5–21	Miocene	52–65	Paleocene		
21–38	Oligocene	65–140	Cretaceous		

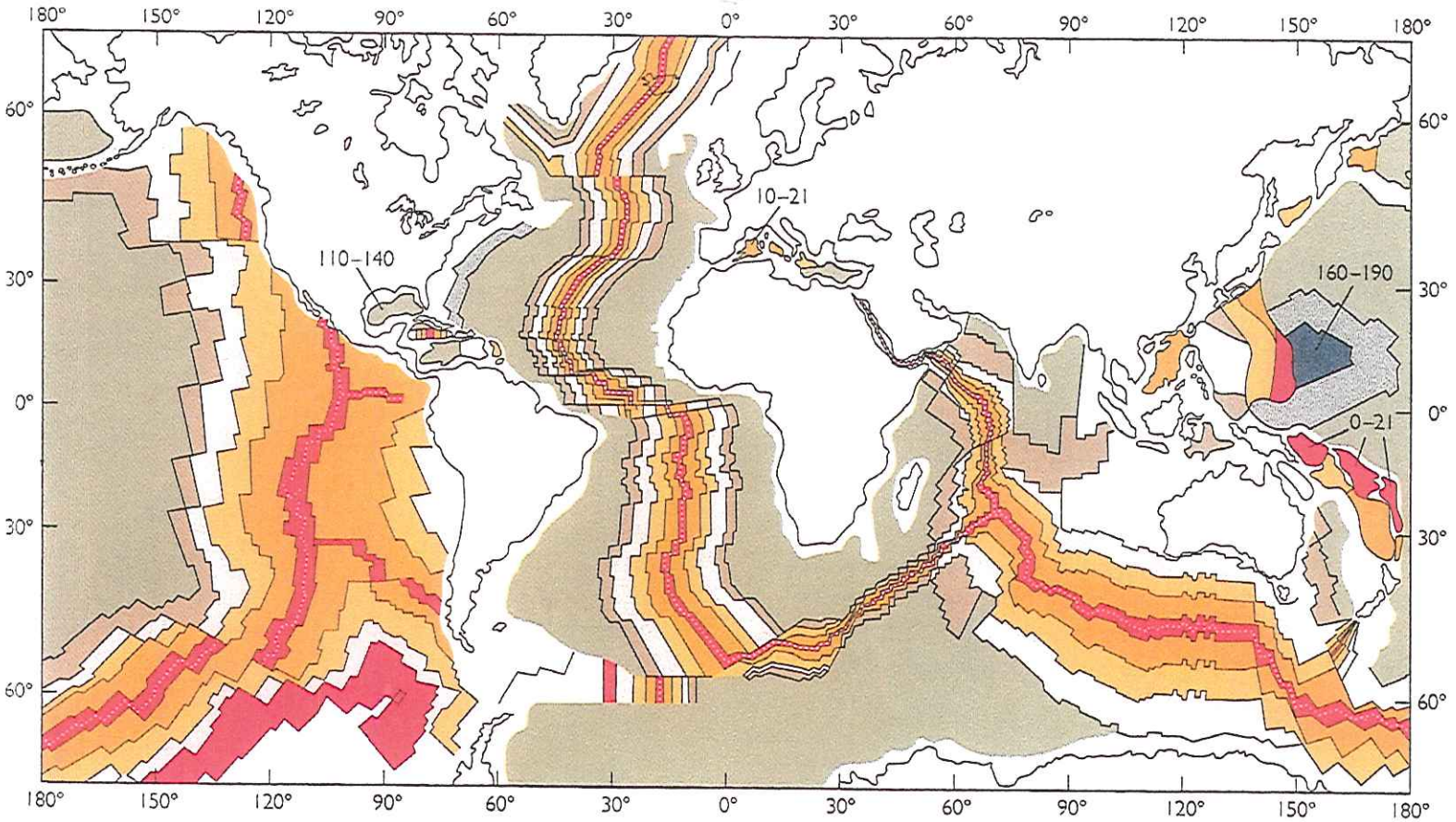

FIGURE 20.11 The worldwide pattern of seafloor spreading is revealed by the isochrons (contours separating the bands of different colors and textures) that give the age of the seafloor in millions of years since its creation at ridges. Mid-ocean ridges, along which new seafloor is extruded, coincide with the youngest seafloor (red). The Atlantic Ocean is symmetrical about the Mid-Atlantic Ridge. Asymmetry of the pattern in the Pacific is caused partly by subduction in the Aleutian Trench south of Alaska, in the Peru-Chile Trench along the west coast of South America, and in many trenches in the western Pacific. (After map prepared by J. Sclater and L. Meinke.)

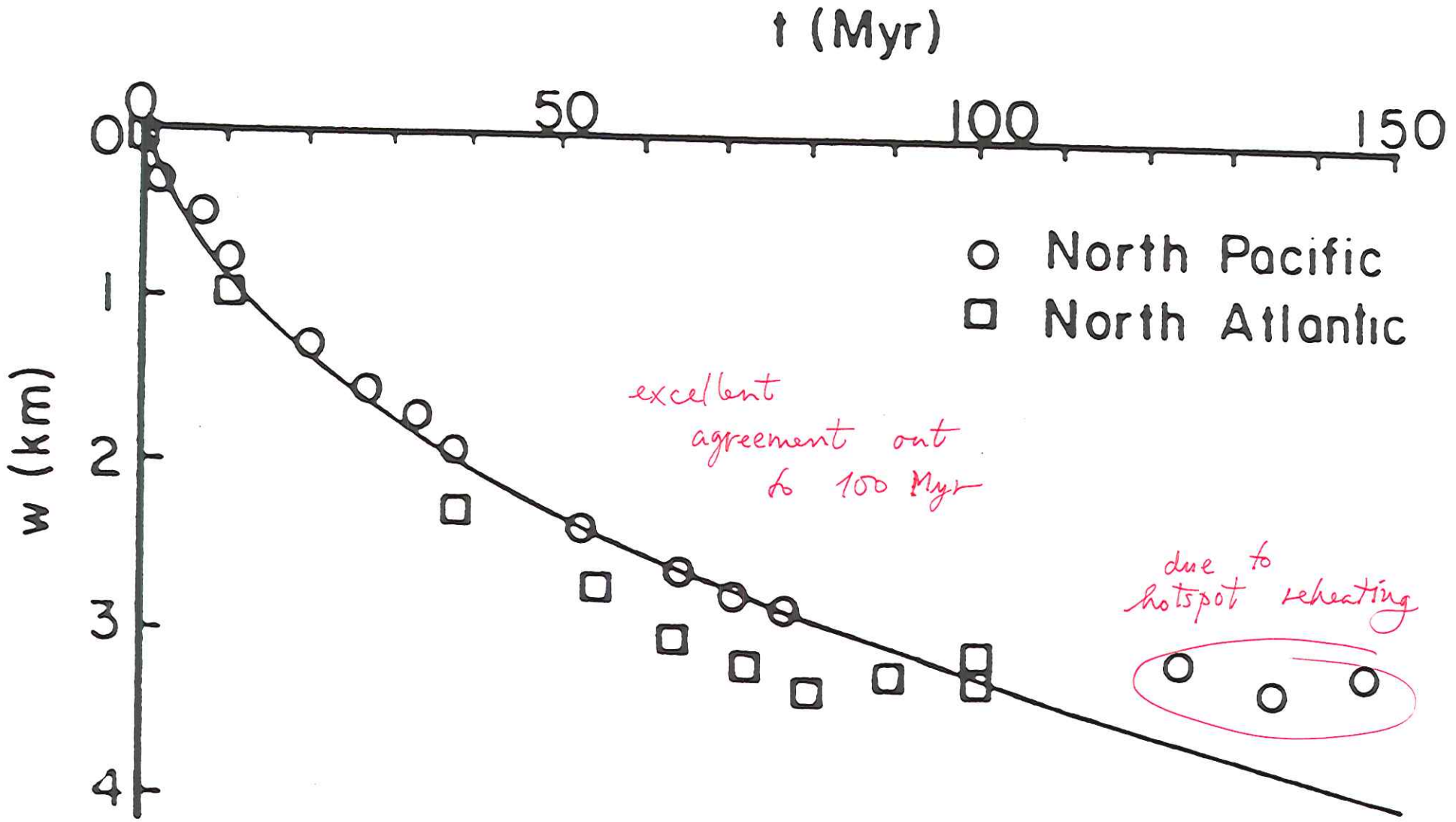
t (Myr)
0
50
100
150
w (km)
1
2
3
4
North Pacific
North Atlantic
excellent agreement out to 100 Myr
due to hotspot reheating

The sediment-corrected depths for ages < 80 m.y. agree very well with the model.

Beyond 80 m.y. the measured depths are slightly shallower.

Debate about the reason for this:

(1) thermal rejuvenation by passage over ascending mantle plumes or "hot spots"

(2) cooling plate (rather than cooling halfspace) model

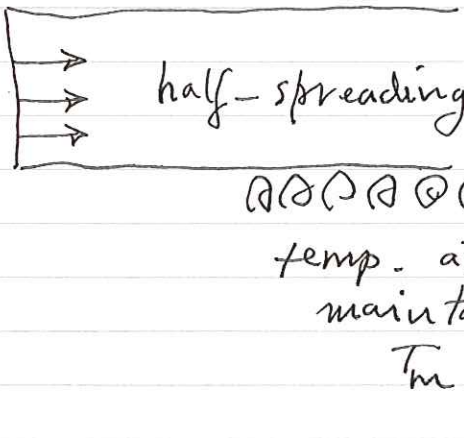

The lithospheric thickness prediction $D = 7\sqrt{t}$ can be compared with seismic measurements.

Find that $D \sim \sqrt{age}$ as predicted.

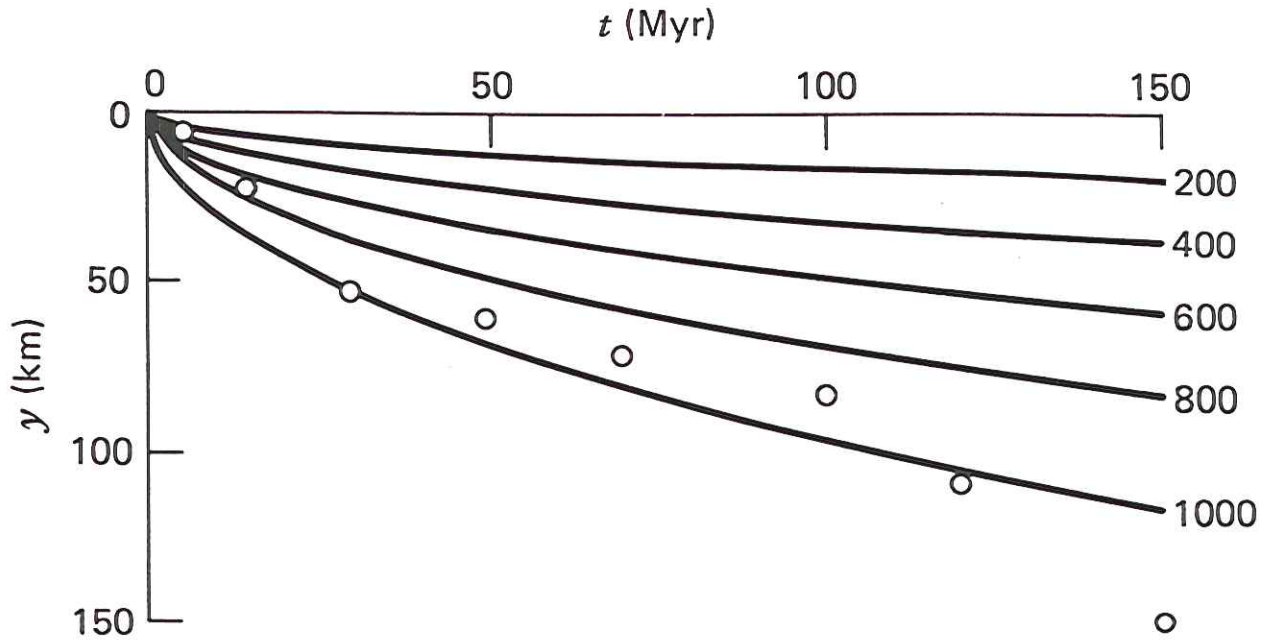

Figure 4-24 The solid lines are isotherms, $T - T_s$ (°K), in the oceanic lithosphere from Equation (4-125). The data points are the thicknesses of the oceanic lithosphere in the Pacific determined from studies of Rayleigh wave dispersion data. (From A. R. Leeds, L. Knopoff, and E. G. Kausel, Variations of upper mantle structure under the Pacific Ocean, *Science*, **186**, 141–143, 1974.)

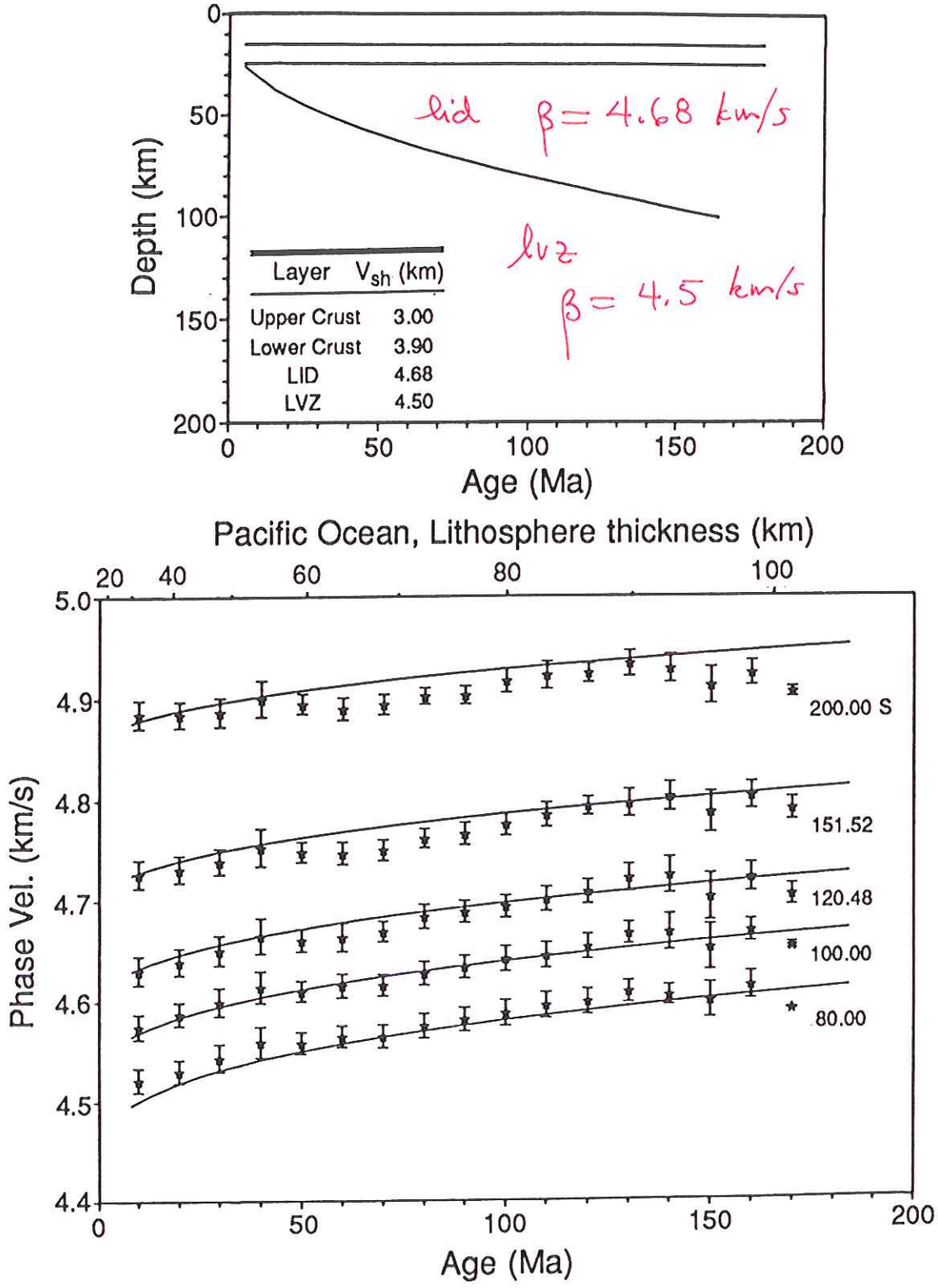

FIGURE 7.32 (Top) A model for lithospheric evolution of shear velocities under the Pacific Ocean. (Bottom) Comparison of the model predictions (solid lines) with observed Love-wave phase velocities with periods from 80 to 200 s plotted as a function of plate age. The observations were obtained by a tomographic inversion of Love waves traversing the Pacific. (From Zhang, 1991.)

EOS

Transactions, American Geophysical Union
Vol. 63 No. 37 September 14, 1982

Cover. The blending of the SYNBAPS U.S. Navy (NORDA) digital bathymetric data from the oceans with the DMA digital terrain elevation data from the conterminous U.S. yields topographic profiles from the west coast of Europe and Africa to the Pacific Ocean. Profiles are shown along latitudes of 31°, 35°, 40°, and 45°N. For the first time the elevation of the Mid-Atlantic Ridge can be compared with that of the Rocky, Appalachian, and Ozark mountains, and the slope east of the Rocky Mountains can be compared to the continental slope off eastern North America. Profiles are shown at 31°, 35°, 40°, and 45°N. For scale reference, depth at 40°N, 60°W is 5045 m. These and other worldwide digital data sets are available from the National Geophysical Data Center. (Photos and information courtesy of Peter W. Sloss, National Geophysical Data Center, Boulder, Colo., and J. R. Heirtzler, Woods Hole Oceanographic Institution, Woods Hole, Mass.).

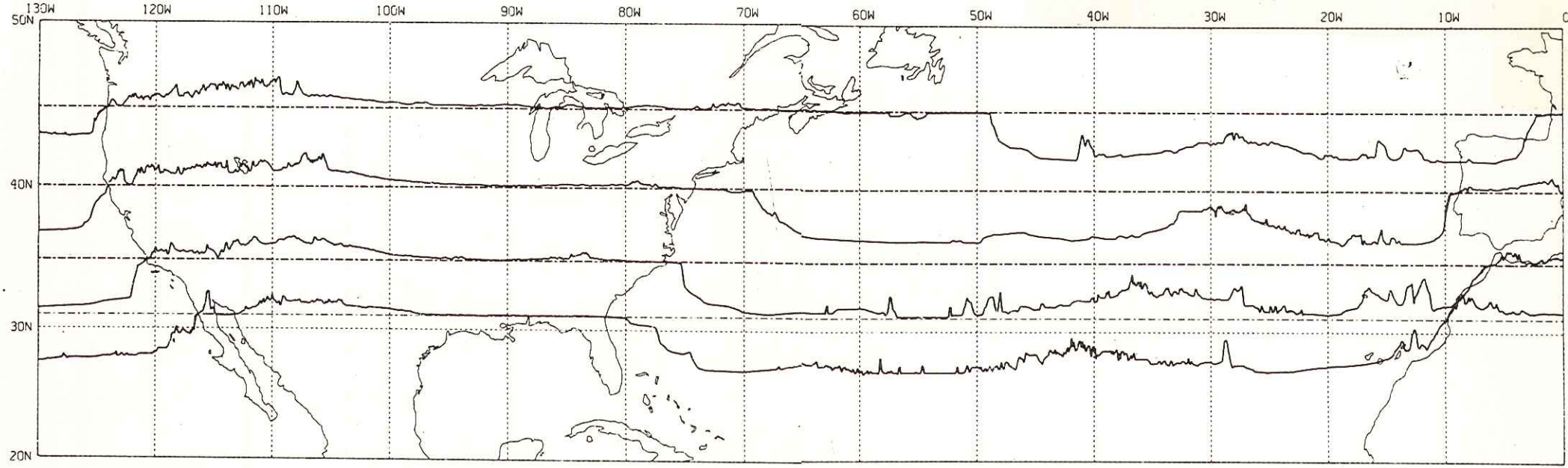

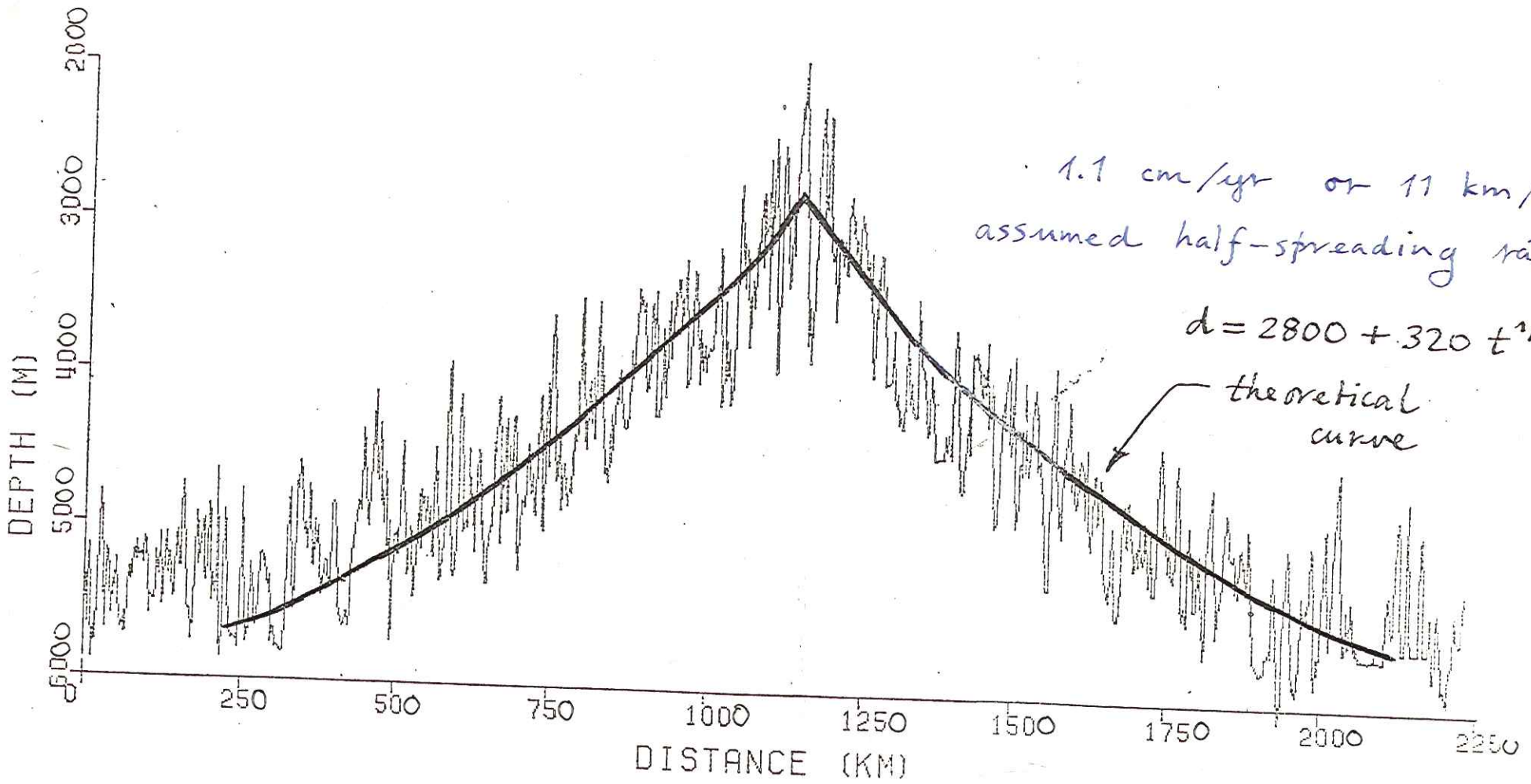
DEPTH (M)
2000
3000
4000
5000
6000
250
500
750
1000
1250
1500
1750
2000
2250
DISTANCE (KM)
1.1 cm/yr or 11 km/m.y.
assumed half-spreading rate
$d = 2800 + 320\, t^{1/2}$
theoretical curve

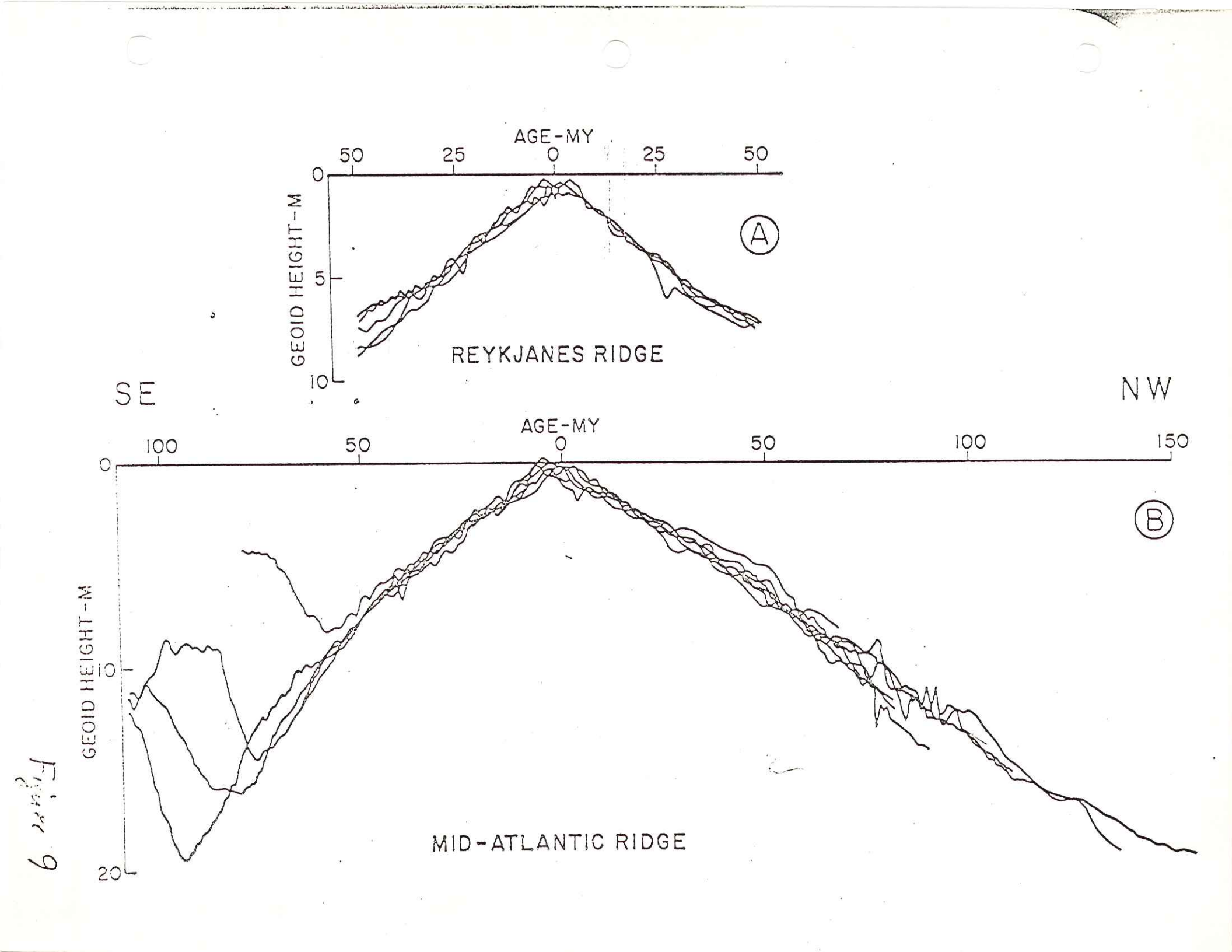
AGE-MY
50
25
0
25
50
0
5
10
GEOID HEIGHT-M
A
REYKJANES RIDGE
SE
NW
AGE-MY
100
50
0
50
100
150
0
10
20
GEOID HEIGHT-M
B
MID-ATLANTIC RIDGE

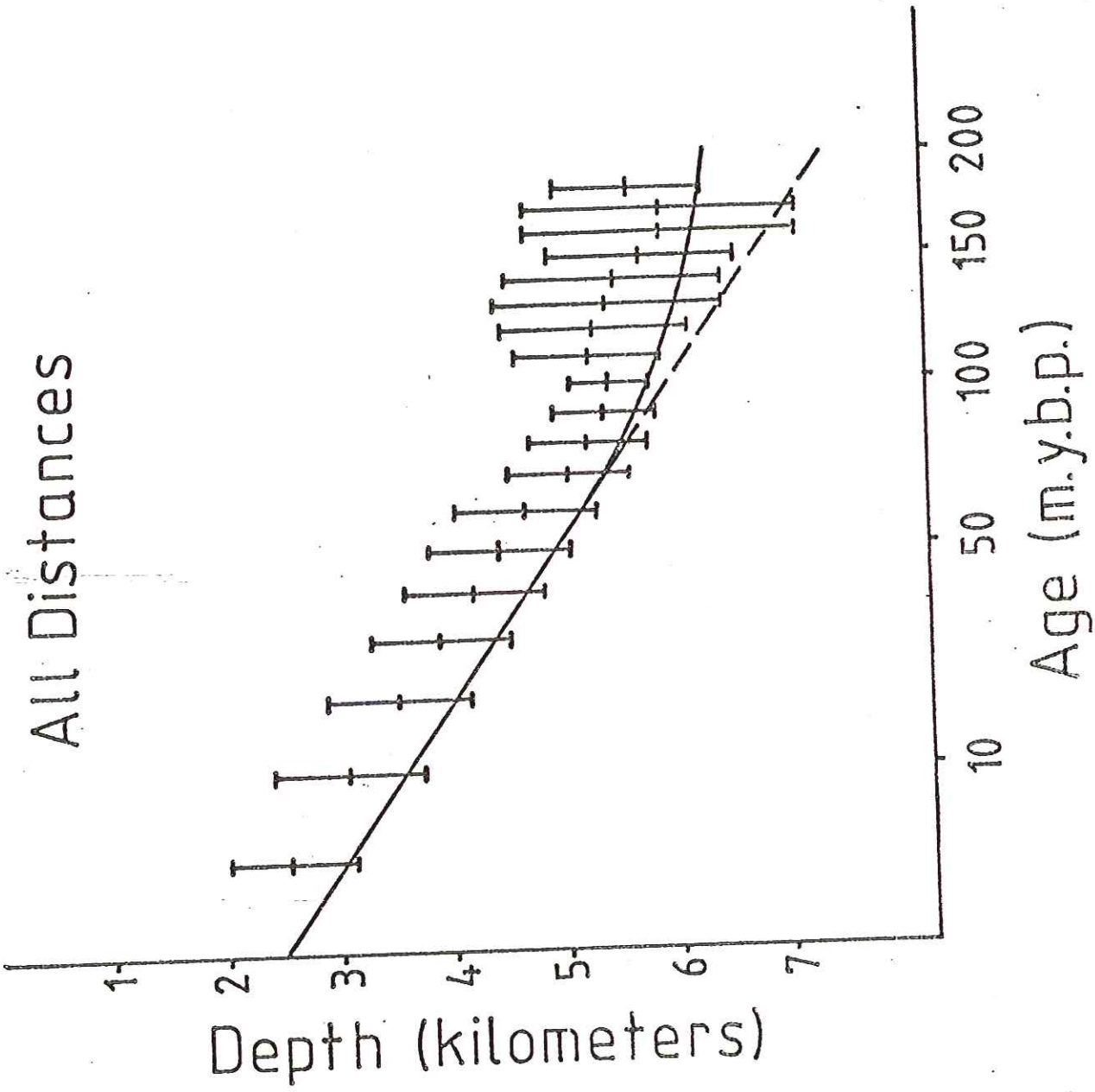

Fig. 7. Seafloor depth versus distance, unsorted by distance from a hotspot track.

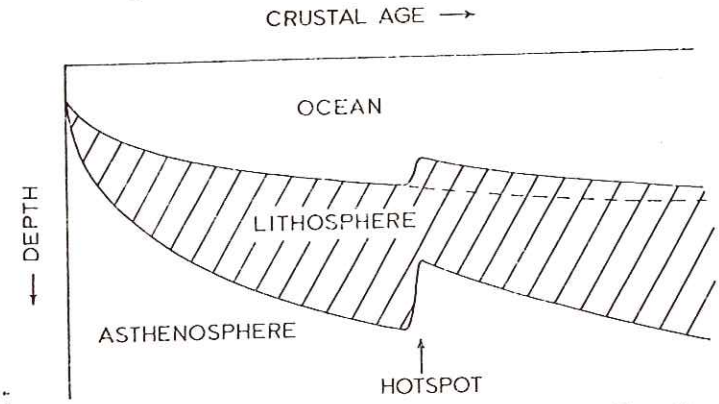

Figure 1. Inferred interaction of the lithosphere with a mid-plate hot-spot. From the ridge to the hot-spot the lithosphere thickens and subsides by cooling. At the hot-spot, extra heat drives the isotherms upwards, thins the lithosphere and causes uplift. Beyond the hot-spot, the lithosphere cools rapidly because it is thin and thus subsides as younger lithosphere at the same depth, rather than as normal lithosphere of the same age (dashed line).

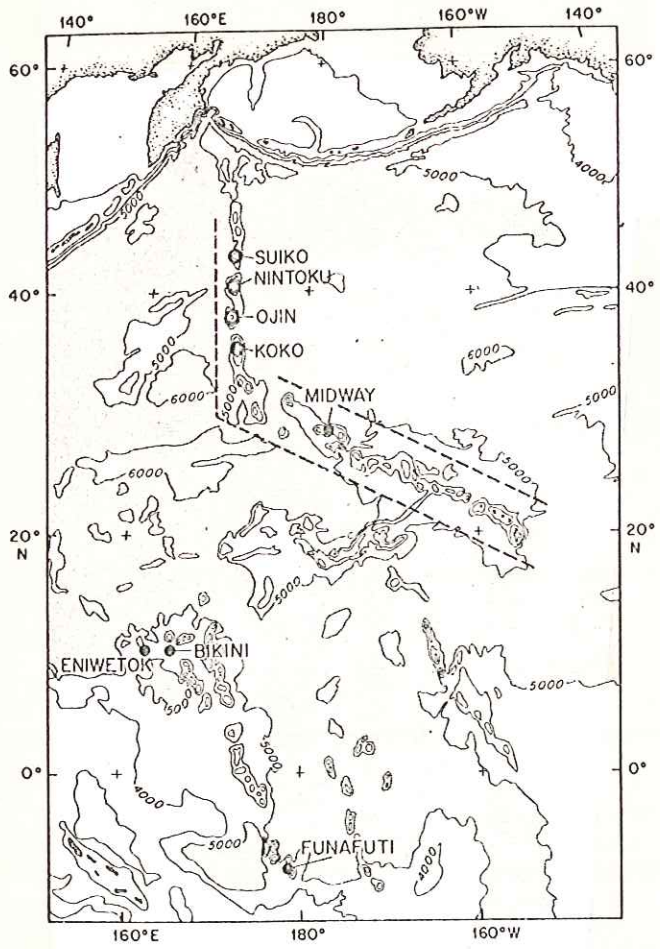

Fig. 1. Bathymetric map of the western Pacific. Solid circles indicate the locations of drilled western Pacific atolls, and open circles the locations of the guyots listed in Table 1. Average depths along dashed lines are plotted in Figure 6.

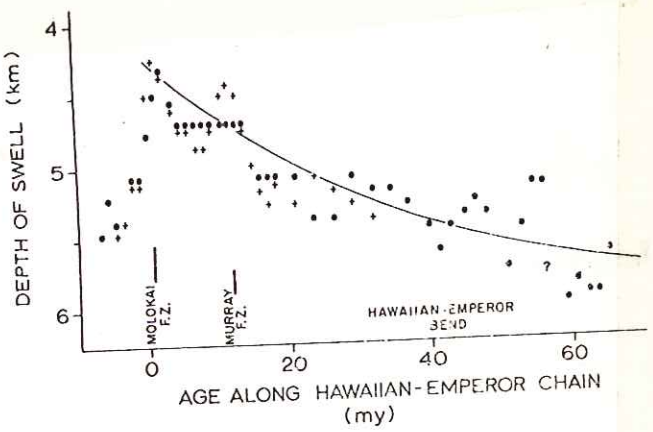

Fig. 6. Depth of the crest of the Hawaiian swell plotted against age along the Hawaiian-Emperor chain (location approximately indicated by dashed lines in Figure 1). Hawaii is assumed to be 0 m.y. old. Age along the chain is taken from Clague and Jarrard [1973], negative ages corresponding to points southeast of Hawaii along the trend of the Hawaiian ridge. Shaded band indicates expected depth if normal age/depth relationship existed in this area. Solid line is empirical age-depth curve for normal oceanic crust between 30 and 100 m.y. old [Parsons and Sclater, 1977].

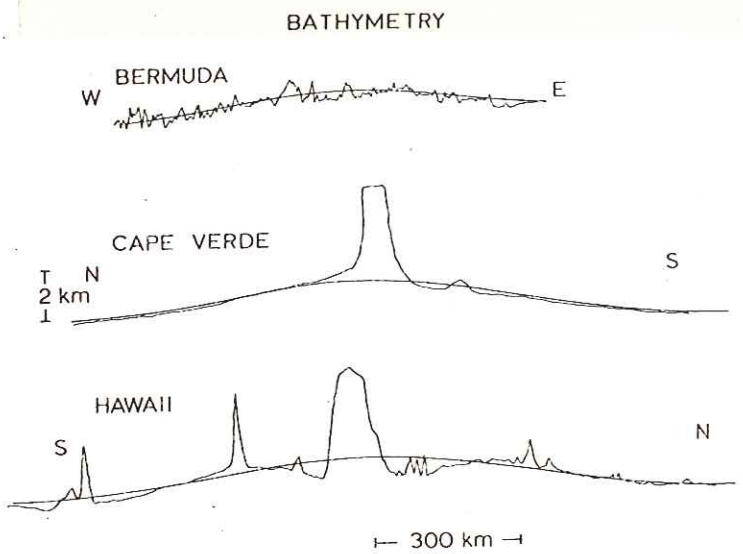

Figure 3. Observed bathymetry of three mid-plate swells, all at the same scale. The smooth curves are the Gaussian representations used with the gravity measurements to infer the depth to the compensation of the swells.

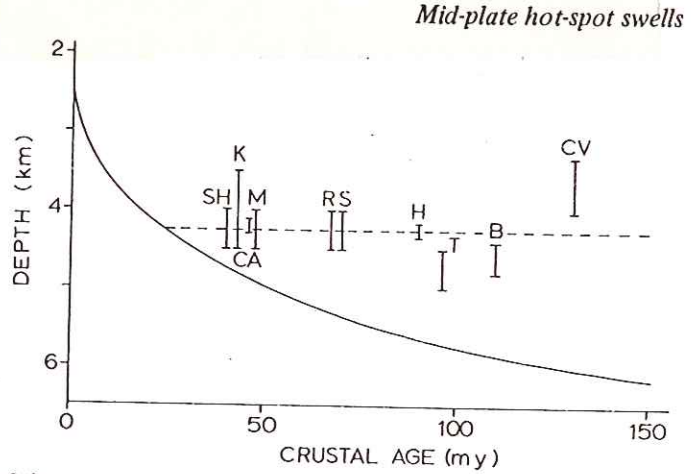

Figure 2. Depth of the crest of mid-plate swells versus the age of the sea-floor on the swell. Solid line is depth–age relation of normal sea-floor. Dashed line is depth of 25 Myr-old lithosphere; most swell crests are at this depth. Symbols and data from Table 1.

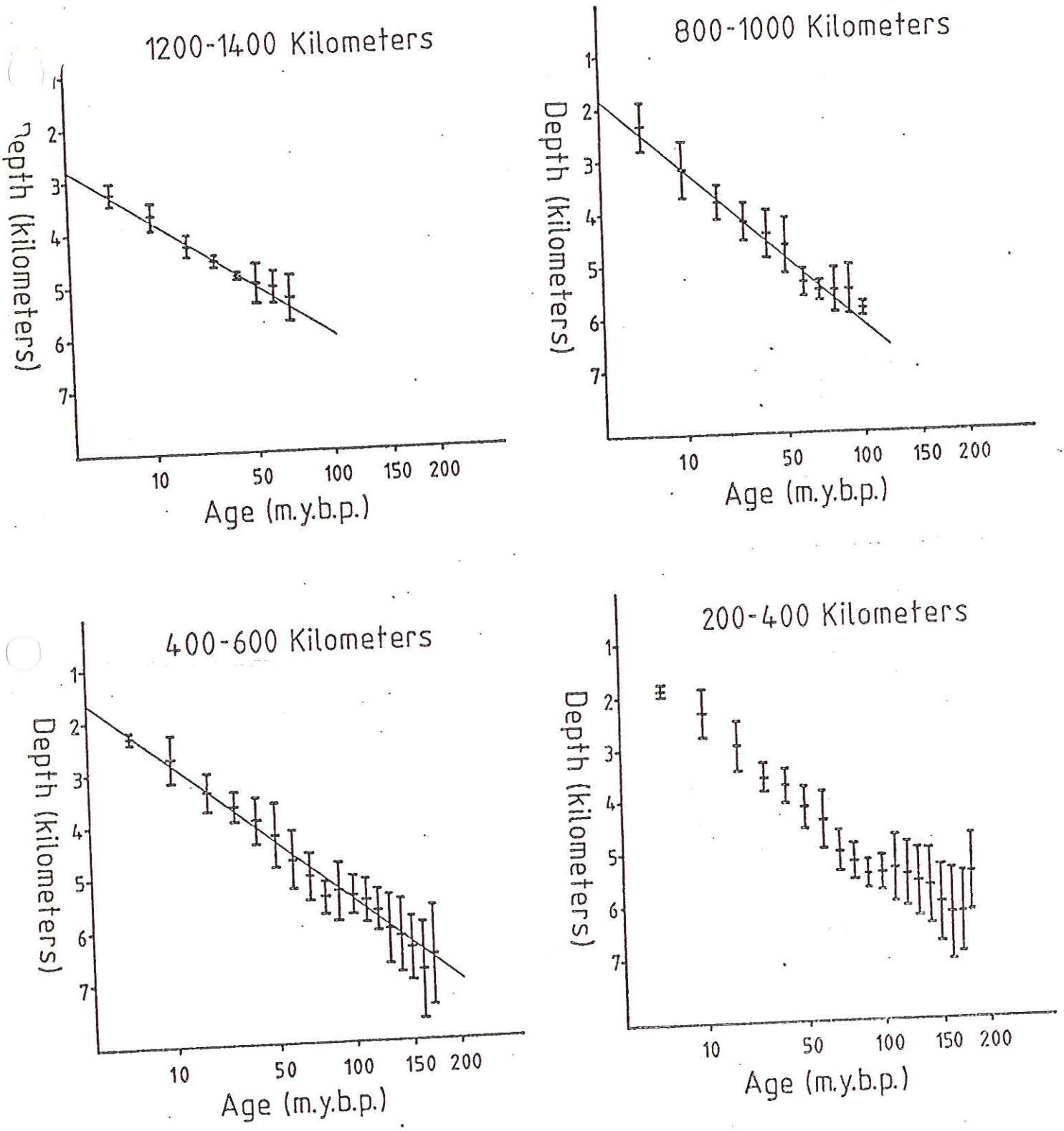

Fig. 6. Seafloor depth versus age for several distance ranges.

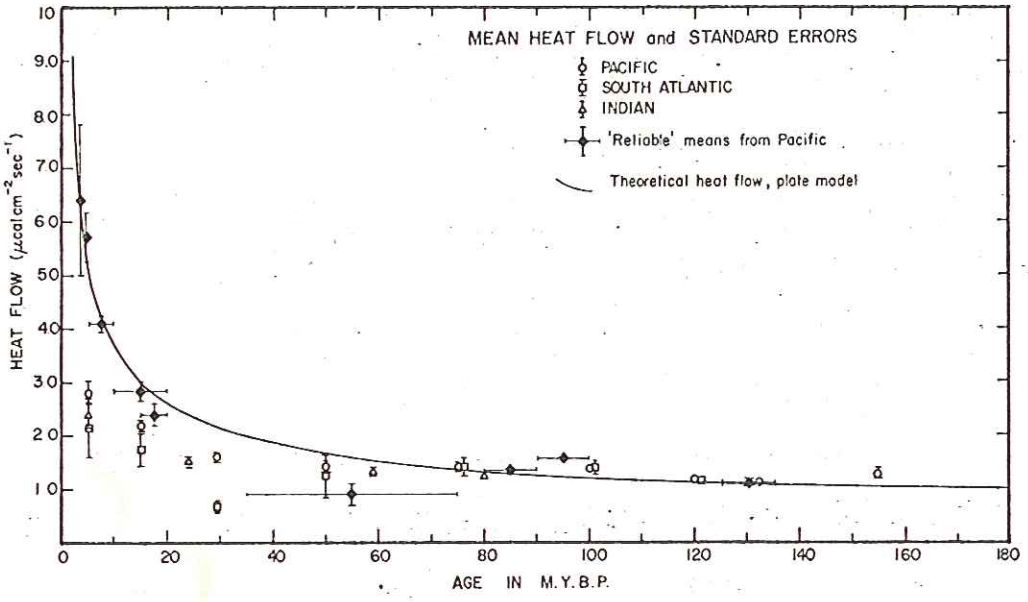

Fig. 10. Standard heat flow averages plus the more selective means of Sclater et al. [1976] plotted as a function of age. The theoretical curve is calculated using the parameters (19) estimated in the text.

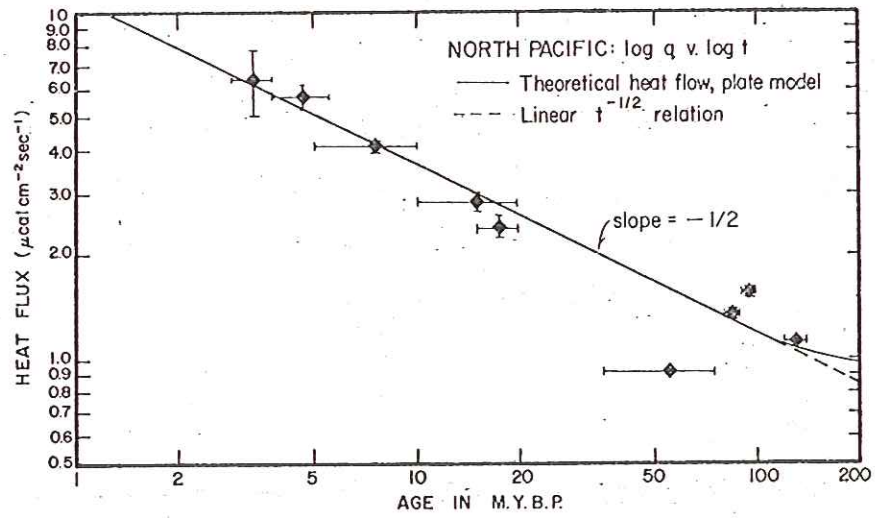

Fig. 11. The reliable heat flow means, calculated using measurements in uniformly well-sedimented areas, plotted on a logarithmic scale versus age and also on a logarithmic scale. The theoretical curve has a slope of -1/2 until an age of about 120 m.y. B.P. The small differences between the plate model values and the continuation of the $t^{-\frac{1}{2}}$ dependence can be seen.

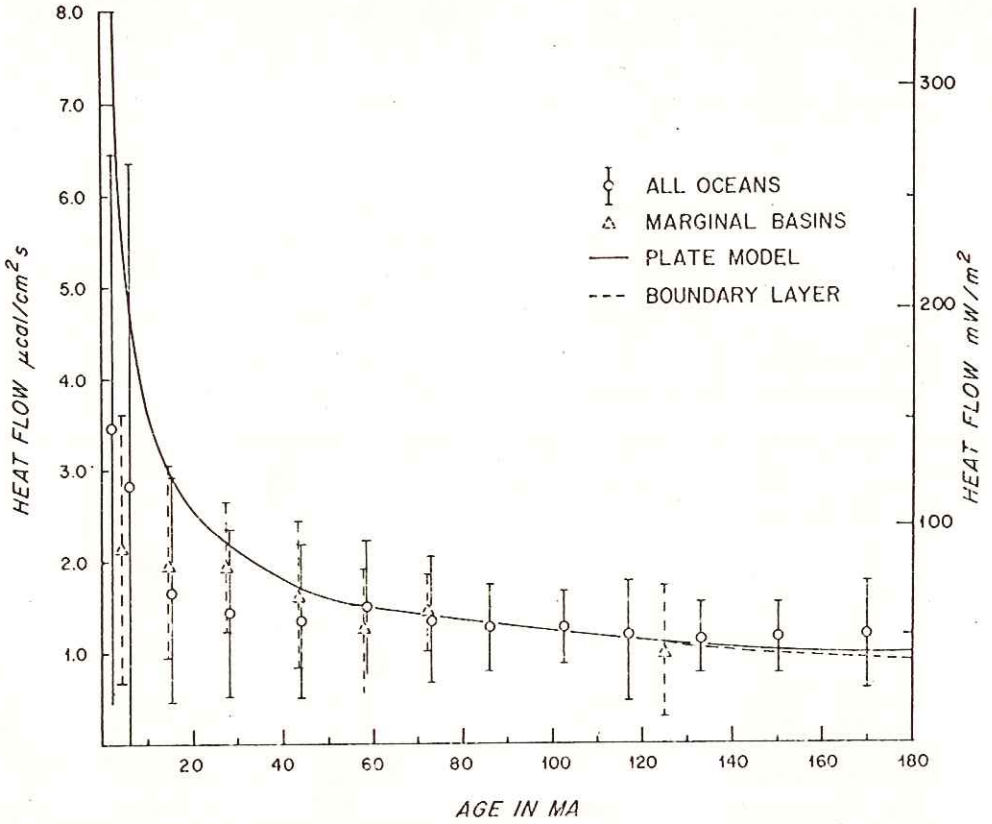

Fig. 4*a*. Mean heat flow and standard deviation for all the oceans and for the marginal basins as a function of age. Also shown are the expected heat flows from the plate and boundary layer models.

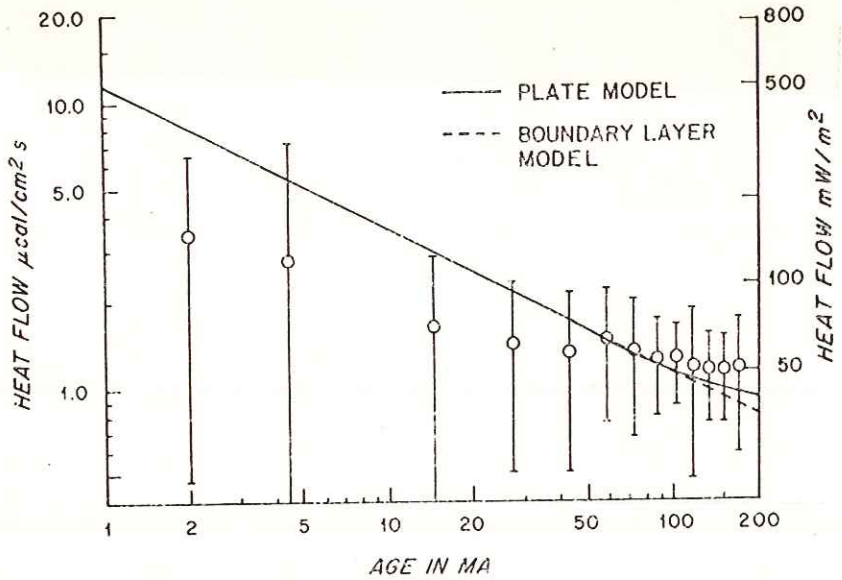

Fig. 4*b*. Log-log plot of the mean heat flow and standard deviation as a function of age for the oceans. Note that for crust younger than 50 Ma the mean values fall below the expected heat flow.

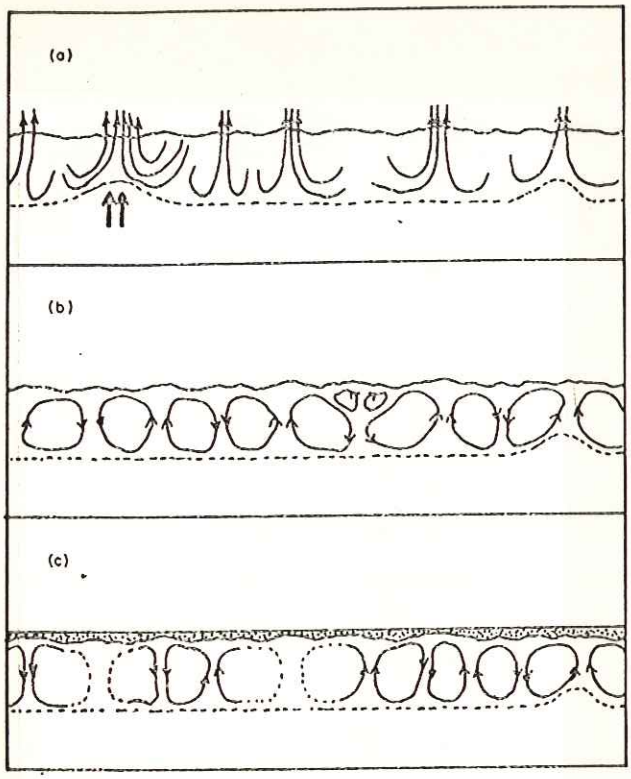

Fig. 6. (*a*) Pattern of convection to be expected near a ridge crest, where the permeable layer is open to the ocean. (*b*) Convective pattern forced by topography in an area of permeable crust bounded by a thin impermeable blanket of sediment. (*c*) The case of permeable crust with a rough boundary, buried by flat-lying sediments. The varying thermal resistance of the sediment blanket overpowers the direct effect of the topography [from *Lister*, 1972].

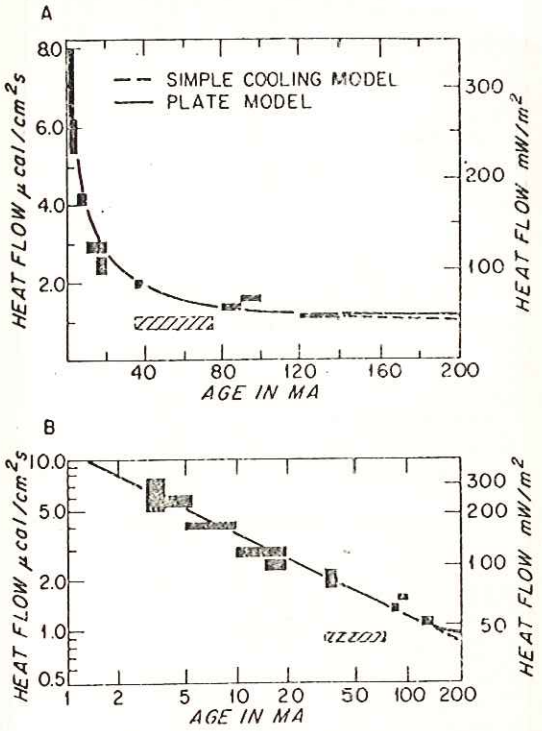

Fig. 9. (*a*) Mean heat flow as a function of age for the well-sedimented areas in the North Pacific and one area in the North Atlantic. Solid rectangles represent the errors in heat flow and age. The solid curve is the theoretical heat flow from the plate model, and the dashed curve that from the boundary layer model. The hatched area represents the value from the equatorial Pacific. (*b*) Log/log plot of heat flow as a function of age for the average values from the well-sedimented areas.

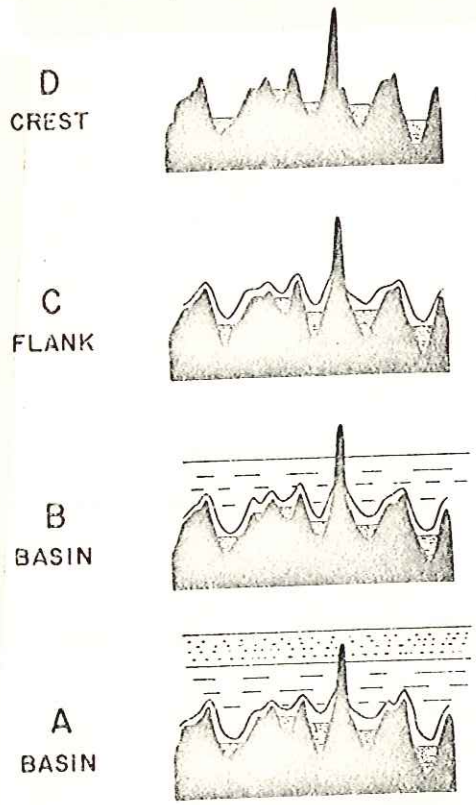

Fig. 7. Schematic diagram of the environmental grades A–D [from *Anderson et al.*, 1977].

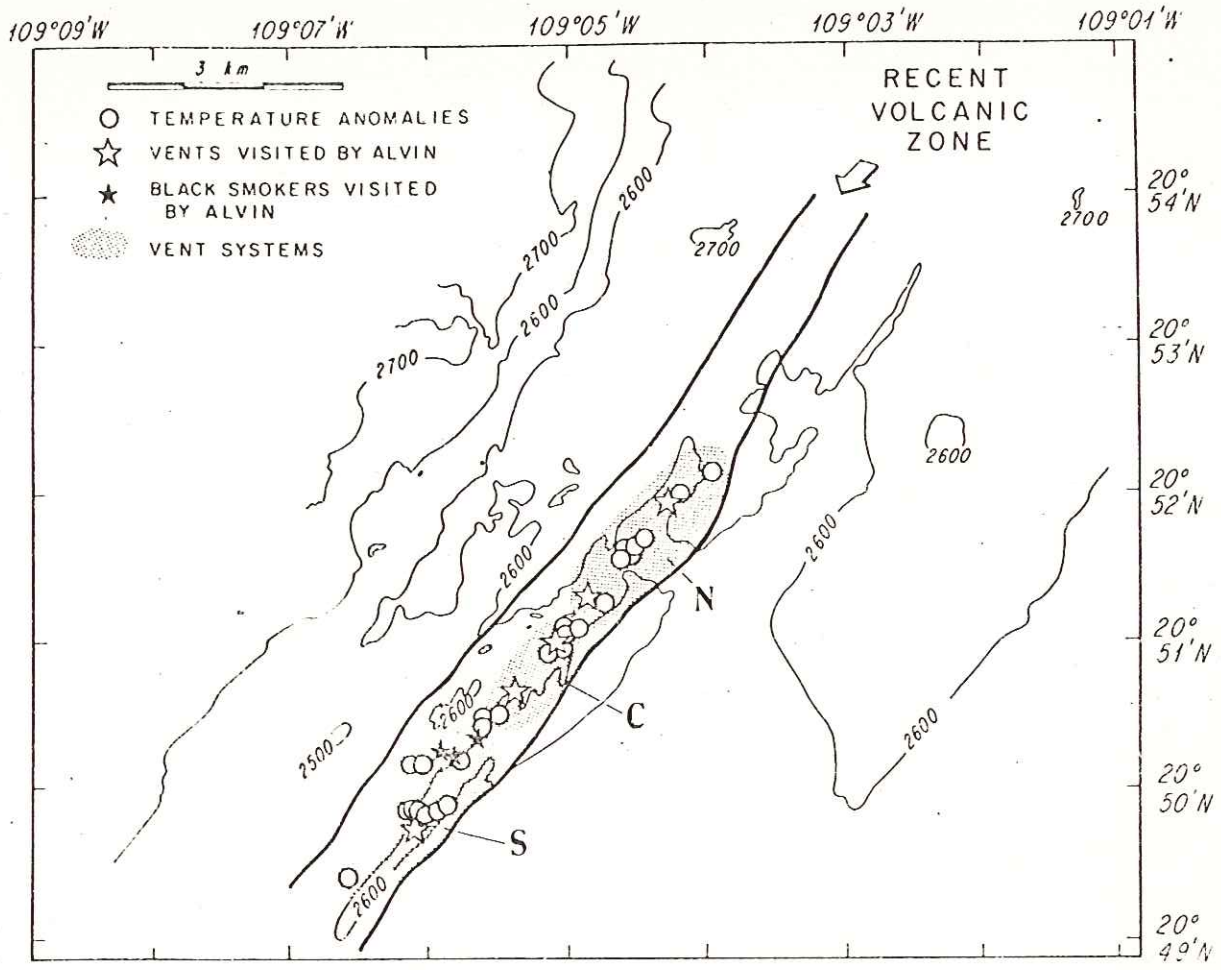

Fig. 2. 100-m contour interval chart from deep-tow mapping. Heavy lines bound the zone of most recent volcanism on the axis. Circles denote hydrothermal sites detected photographically and thermally from ANGUS, stars show vents visited by "Alvin", solid stars are the three black smoker vent fields studied from "Alvin". The three major vent systems (northern, central, southern) are outlined. Note that the active vent system lies entirely within the zone of recent volcanism within a band only 200–500 m wide.

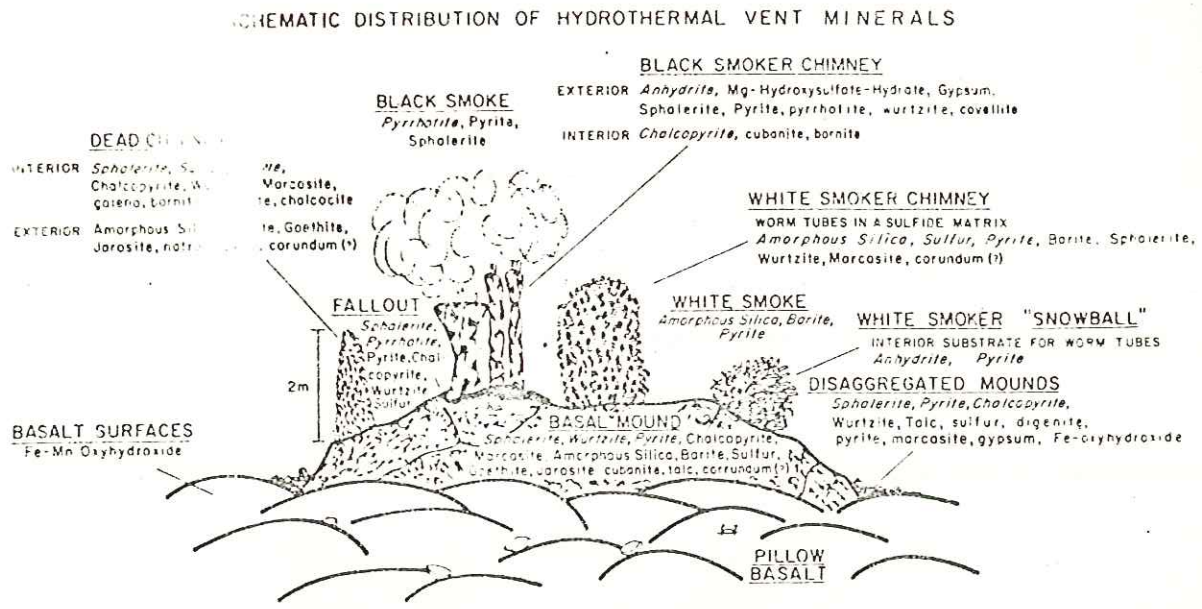

Fig. 10. A composite sketch illustrating the variety of structures observed at the different RISE vent sites and the mineral distributions associated with these structures. Note that anhydrite and Mg-hydroxysulfate-hydrate are found only in active, black smokers, and pyrrhotite occurs mainly in black smoke or in black fallout sediment. Note also that Mn-oxyhydroxides precipitate on basalt surfaces slightly away from vents. Main phases are italicized; minor phases are capitalized; accessory phases are printed in lower case.

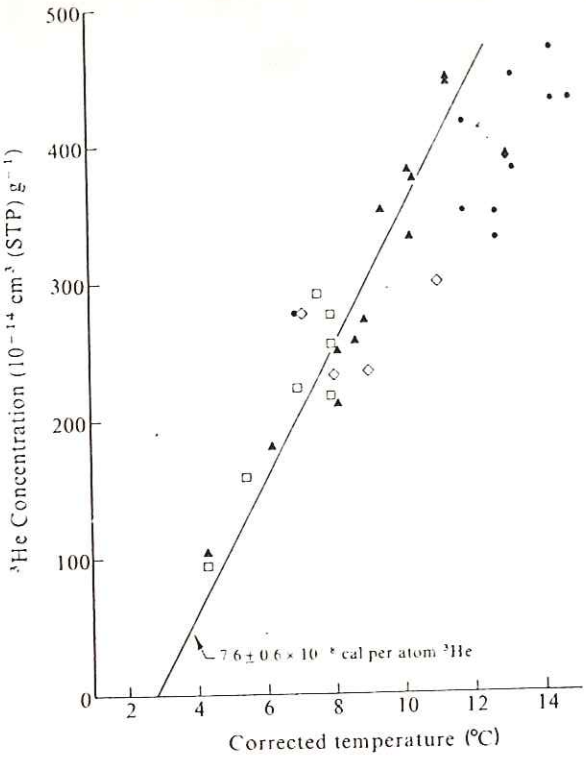

Fig. 2 The samples, exclusive of Garden of Eden, exhibit a tight correlation between excess ^{3}He and temperature (σ (T) $\approx$ 0.7 °C), with a slope of 7.6×10^{-8} cal per atom. Exclusive of the Garden of Eden samples (see text). Note the substantial and systematic offset of the Garden of Eden samples. Vent areas as in Fig. 1.

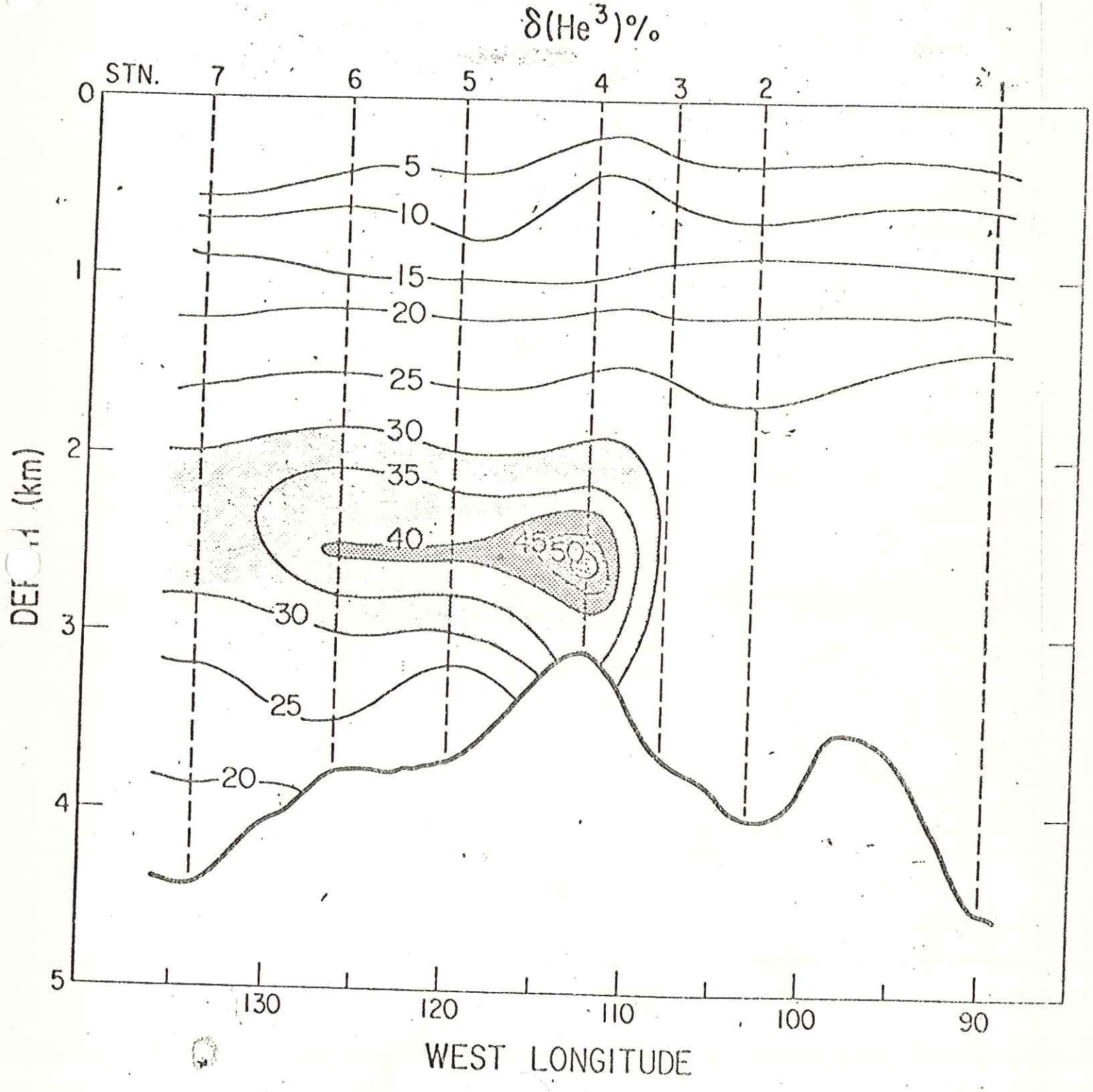
δ(He³)%
STN.
7
6
5
4
3
2
0
1
2
3
4
5
DEPTH (km)
5
10
15
20
25
30
35
40
45
50
30
25
20
130
120
110
100
90
WEST LONGITUDE